AN INVESTIGATIONS INTO THE MICRO WIRE ELECTRICAL DISCHARGE MACHINING OF SHAPE MEMORY ALLOY

THE GRADUATE SCHOOL OF NATURAL AND APPLIED SCIENCES
OF
ATILIM UNIVERSITY

HASSAN ALI M. MESHRI

A MASTER'S THESIS
IN
THE DEPARTMENT OF MANUFACTURING ENGINEERING

DECEMBER 2019

AN INVESTIGATIONS INTO THE MICRO WIRE ELECTRICAL DISCHARGE MACHINING OF SHAPE MEMORY ALLOY

A THESIS SUBMITTED TO
THE GRADUATE SCHOOL OF NATURAL AND APPLIED SCIENCES
OF
ATILIM UNIVERSITY

BY

HASSAN ALI M. MESHRI

IN PARTIAL FULFILLMENT OF THE REQUIREMENTS
FOR
THE DEGREE OF MASTER OF SCIENCE
IN
THE DEPARTMENT OF MANUFACTURING ENGINEERING

DECEMBER 2019

Approval of the Graduate School of Natural and Applied Sciences, Atılım University.

_____

Prof. Dr. Ali Kara

Director

I certify that this thesis satisfies all the requirements as a thesis for the degree of Master of science in Manufacturing Engineering Department, Atilim University.

_____

Prof. Dr. Sadık Engin Kılıç

Head of Department

This is to certify that we have read the thesis AN INVESTIGATIONS INTO THE MICRO WIRE ELECTRICAL DISCHARGE MACHINING OF SHAPE MEMORY ALLOY submitted by HASSAN ALI M MESHRI and that in our opinion it is fully adequate, in scope and quality, as a thesis for the degree of Master of Science.

_____	_____
Prof. Dr. Sadık Engin Kılıç	Asst. Prof. Dr. Samet Akar
Co-Supervisor	Supervisor

Examining Committee Members:

Asst Prof. Dr. Dr. Şehram Dizeci
Mechanical Eng. Department, Ted University _____

Asst. Prof. Dr. Samet Akar
Mathematics Eng. Department, Atilim University _____

Asst. Prof. Dr. Bahram Lotfi Sadigh
Manufacturing Eng. Department, Atilim University _____

Date: 20 DECEMBER 2019

I hereby declare that all information in this document has been obtained and presented in accordance with academic rules and ethical conduct. I also declare that, as required by these rules and conduct, I have fully cited and referenced all material and results that are not original to this work.

Name, Last name: HASSAN ALI M MESHRI

Signature:

ABSTRACT

AN INVESTIGATIONS INTO THE MICRO WIRE ELECTRICAL DISCHARGE MACHINING OF SHAPE MEMORY ALLOY

Meshri, Hassan Ali

M.S., Manufacturing Engineering Department

Supervisor: Asst. Prof. Dr. Samet Akar

Co-Supervisor: Prof. Dr. Sadık Engin Kılıç

December 2019, 78 pages

Recently, the use of nitinol as a shape memory alloy (SMA) has become significant in vital industries, such as the medical and aerospace industries, due to its distinctive characteristics of pseudoelasticity and shape memory effect. Due to its high hardness, high fracture toughness, strain hardening and issued such as rapid tool wear the use of conventional machining processes has become difficult when producing complex shapes from nitinol. Therefore, non-traditional machining processes, especially wire electro-discharge machining (WEDM) has become the dominant method of machining nitinol alloy. However, WEWD faces some challenges, especially in terms of surface integrity of the workpiece which requires an in-depth investigation. In this study, the effect of μ-WEDM process on nitinol alloy was studied. 100 μm diameter brass wire was used for the cutting in addition to a set of μ-WEDM adjustable input cutting parameters, such as peak current (Ip), servo voltage (Sv), pulse on time (T_{on}), and pulse off time (T_{off}) are selected. The experiments were designed based on L27 Taguchi orthogonal array to reduce the number of experiments. Multi-regression analysis was applied based on the surface response methodology (RSM) to determine the effect of μ-WEDM process parameters on the surface integrity of the nitinol alloy. The aim of surface integrity studies was to minimizing Kerf width variation, minimizing white layer thickness (WLT), maximizing metal removal rate (MRR), minimizing surface roughness (Ra), and minimizing μ-hardness. Optimization studies were performed using two algorithms, the gradient algorithm (GA) and the particle swarm optimization algorithm (PSO) to determine the best μ-WEDM cutting parameters set for each output parameter individually according to the target that was specified. Moreover, a combined multi-response optimization analysis was performed to find the best set of μ-WEDM process parameters to achieve the best surface integrity of the nitinol alloy sample that satisfies the goal of all output responses' simultaneously.

Keywords: μ-WEDM, Nitinol, WLT, MRR, KERF, Surface roughness, hardness, RSM, PSO.

ÖZ

ŞEKİL HAFIZALI ALAŞIMININ MİKRO TEL ELEKTRİK EREZYON YÖNTEMİ İLE İŞLENMESİNİN ARAŞTIRILMASI

Meshri, Hassan Ali

Yüksek Lisans, İmalat Mühendisliği Bölümü

Tez Yöneticisi: Dr. Öğr. Üyesi Samet Akar

Ortak Tez Yöneticisi: Prof. Dr. Sadık Engin Kılıç

2019, 78 sayfa

Son zamanlarda, nitinol alaşımının (ŞHA) kullanımı, tıbbi ve havacılık endüstrileri gibi hayati endüstrilerde, yapay esneklik ve hafıza şekli gibi ayırt edici özellikleri nedeniyle önemli hale gelmiştir. Bu özelliklerin bir sonucu olarak, geleneksel işleme yöntemlerinin kullanımı, karmaşık şekilli nitinollerin üretimini zorlaştırmıştır. Bu nedenle, Mikro Elektro Erezyon yöntemi, nitinol alaşımı işlemede baskın ve geleneksel olmayan yöntemi haline gelmiştir. Mikro Elektro Erezyon işleme yönteminin nitinol alaşımı üzerindeki etkisi çalışılmıştır. Maksimum akım (Ip), servo voltaj (Sv), darbe süresi (T_{on}) ve darbe düşme süresi (T_{off}) gibi değiştirilebilir giriş kesme parametreleri seçilerek 100 çapında pirinç tel kullanılarak işleme yapıldı. Deneyler, deneme sayısını azaltmak için L27 Taguchi dikey sıralar temel alınarak tasarlanmıştır. Yüzey tepki yöntemi işlem parametrelerinin nitinol alaşımlı numunelerin yüzey bütünlüğü üzerindeki etkilerini belirlemek için Mikro Elektro Erezyon yöntemi kullanılarak çoklu bağlanım yöntemi uygulandı. Nitinol numuneleri üzerinde çalışılan yüzey bütünlüğü parametreleri, Kerf genişlik değişimini, beyaz tabaka kalınlığını, metal kaldırma oranını, yüzey pürüzlülüğünü ve mikro sertliği en aza indirmektedir. Optimizasyon analizleri, iki farklı algoritma gradyan ve parçacık sürüsü optimizasyon algoritmaları kullanılarak, her bir çıkış parametresi için belirlenen hedefe göre ayrı ayrı ayarlanan Mikro Elektro Erezyon yöntemi en iyi kesme parametrelerini belirlemek için yapıldı. Dahası, Nitinol alaşımlı numunenin en iyi yüzey pürüzlülüğü için ayarlanan Mikro Elektro Erezyon kesme parametresini bulmak için birleştirilmiş çoklu yanıt optimizasyon analizi tüm çıktı yanıtlarının hedefini aynı anda karşılamaktadır.

Anahtar Kelimeler: Mikro Elektro Erezyon, Nitinol, WLT, MRR, Kerf Width, Ra, Mikro sertlik, RSM, PSO.

To My Parents

ACKNOWLEDGMENTS

I give thanks to God, who enabled me to research such a contentious issue these days, and for lighting my way through the path of science.

I would like to offer my supervisor Asst. Prof. Dr. Samet Akar my sincere appreciation for his great assistance, guidance and excellent support during the thesis period. Indeed, this work would not have been possible without his great support and unlimited efforts.

I extend my deep appreciation to my co-supervisor Prof. Dr. Sadık Engin Kılıç for his guidance, patience, support, and encouragement.

I would like to thank Assoc. Prof. Dr. Yiğit Karpat and Dr. Şakir Baytaroğlu at the Micro System Design and Manufacturing Center of Bilkent University for their help in surface roughness and micro-hardness measurements.

I would like to thank Assoc. Prof. Dr. Seha Tirkeş and Asst. Prof. Dr. Salih Ertan for Chemical Engineering and Applied Chemistry department of Atilim University for their support in preparing various etching solutions for microstructure analysis of Nitinol.

I would like to thank my wife Huda Berber and my children for their love and encouragement.

I would like to thank all of those who continued to support and encourage me to complete this thesis.

Finally, my heartfelt warm greetings to my parents, Ali Meshri and Suad Kara, for their love and support for me throughout my life.

TABLE OF CONTENTS

LIST OF TABLES

LIST OF FIGURES

LIST OF ABBREVIATIONS

SMA	-	Shape Memory Alloy
μ-WEDM	-	Micro Wire Electrical Discharge Machining
SME	-	Shape Memory Effect
PE	-	Pseudoelasticity
GA	-	Gredient Algorithm
PSO	-	Particle Swarm Optimization
Sa	-	Arithmetic Average Height
W.L.T	-	White Layer Thickness
MRR	-	Metal Removal Rate
μ-hardness	-	Microhardness
Ip	-	Peak Current
Sv	-	Servo Voltage
Ton	-	Pulse On Time
Toff	-	Pulse Off Time
CD	-	Combined Desirability Index
Id	-	Individual Desirability Index

CHAPTER 1

Introduction

1.1 Introduction

Nitinol an equiatomic nickel-titanium alloy has become one of the most important shape memory alloys (SMAs) currently used in medical, aerospace and other industrial fields. It was introduced with a shape memory effect in the US Naval Ordinance Laboratory (NOL) in 1960 by Buehler et al. [1]. Some uses include orthodontic equipment, microelectromechanical systems (MEMS), sensor and actuators [2]. Nitinol is used because of its high strength at moderate and low temperatures as well as its high corrosion and wear resistance, high ductility, good fatigue life, and high bio-compatibility [3].

Nitinol alloy has more unique microstructural properties than other alloys. Nitinol has two phases: martensite at low temperatures and austenite at high temperatures. Under the influence of external, Nitinol can move from the martensite phase to the austenite phase and vice versa if these external effects are removed. Martensite and austenite are two different crystal structures or phases in NiTi alloys [4, 5].

The metamorphosis phase gives Nitinol a unique characteristic among other alloys, namely the shape memory effect and pseudoelasticity behaviors (SE) [6]. The effect of SME and SE on Nitinol alloy makes it return to its original form with a high reactivity (approx. 8%). SME causes a transformation of the martensite phase to the austenite phase due to thermal or mechanical loads [7, 8].

Figure 1 shows the different phases of the Nitinol alloy (SMA). Nitinol initially at the origin point O in a complete austenitic state. Without applying stress, if the Nitinol is

cooled along path O-A below the martensite finish temperature “Mf”, a complete transformation from the austenite phase to a twinned martensite phase will occur. Through path A-B, if loads are applied, the material will deform into a reoriented de-twinned martensite. Then, unloading onto path B-C will cause elastic unloading of the reoriented de-twinned martensite. However, the material stays deformed and pseudoplastic. While heating path C-D to the austenite finish temperature (Af), the material transforms from martensite to austenite and recovers from the deformation to its former shape, the ‘shape memory effect’. In the complete austenitic phase above the austenite finish temperature (Af), Nitinol can be loaded along through the path O-E transformation and a martensitic state will occur. A large elastic strain of up to 11% can be achieved. Through path E-O while unloading, the martensitic phase will transform back to the austenitic phase and the super-elastic deformation will be recovered, showing a hysteresis loop in the stress-strain diagram [6, 9].

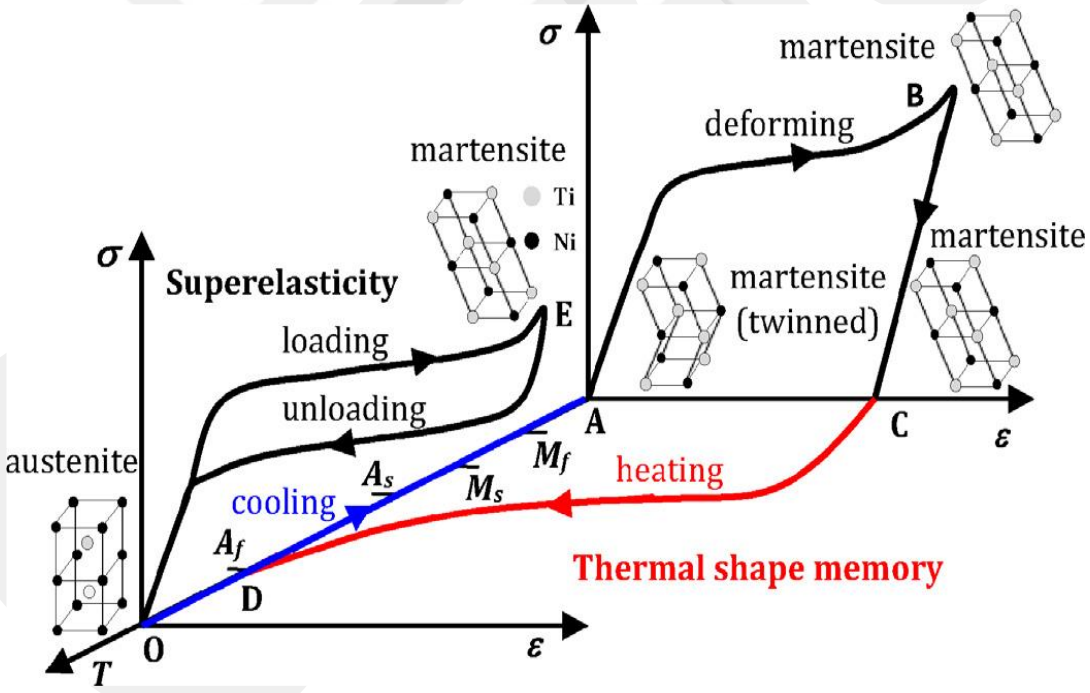

Figure1. 1 Different phases of a shape memory alloy (Nitinol alloy) [6].

The ability of SMA to recover from large strain due to mechanical or thermal loads has made them important alloys used in many vital industries, such as then petroleum, biomedical and aerospace industries [10-13].

Nitinol alloy with near-equiatomic compositions is the most well-known shape memory alloy. As the nickel content increases in the alloy, the transformation temperature will decrease. The martensitic phase is known as the low-temperature phase having a monoclinic crystalline structure. In contrast, the austenitic phase, known as the high-temperature phase, has a body-centered cubic crystalline structure [14].

Depending on the SME (shape memory effect) characteristic of the Nitinol alloy, the behavior of this alloy can be trained in two ways depending on the memorability. In the first type, which is known as one-way shape memory (OWSM), the sample is cooled to below the temperature of the Mf and then deformed into a planned shape, as in Figure 1.2. The sample is then reheated to a higher temperature than Af until it is fully austenitic. This method needs to be repeated 20 to 30 times. Thus, the sample will acquire its planned shape by cooling below the Mf and it will return to its austenitic shape by heating to above Af. In the second type, which is known as two-way shape memory (TWSM), the sample is bent or formed exactly at above Ms temperature to make reference characters for the martensitic phase by the applied stress, followed by it being cooled to below Mf temperature, and then reheated to above Af. The sample will acquire its shape in the austenitic phase [15].

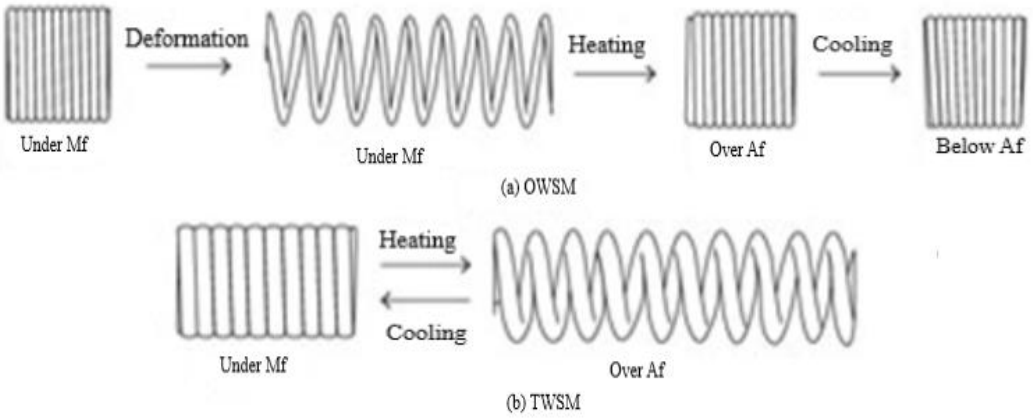

Figure1. 2 one-way and two-way memory training [15]

The machinability for Nitinol alloy has become an important concept in a number of fields of industry nowadays. The conventional machining methods of this alloy leads to high tool wear and low machined surface quality of products, which has become noticeable, due to the effect of high toughness, their higher strain hardening effect, and pseudoelasticity behavior. As a result of difficulties in cutting through conventional methods [16, 17]. new research has been developed and researchers have attempted to discover a number of solutions to improve the ability to manufacture items using unconventional methods [18].

Widely used of Wire-EDM in cutting conductive materials. By creating controlled electric sparks between electrode “wire” and anode “workpiece”. These dense high-energy sparks melt and vaporize the material on the workpiece surface [19].

Dielectric fluid is used in this process. Dielectric fluid is flushed between the electrode wire and the anode workpiece to remove the particles which were produced during the cutting process and to prevent these particles from oxidizing and re-solidifying on the workpiece surface and cutting wire [20, 21].

1.2 Literature Review

The melting temperature and thermal conductivity of the shape memory alloys are two major factors affecting the metal removal rate (MRR). When the thermal conductivity is high, the heat transfers of the remainder of the bulk material adjacent to the machined surface is faster. This leads to a decrease in the metal removal rate. Increasing the spark energy by increasing the peak current leads to an increase in the rate of melting and evaporation of the eroded material, and increasing the pulse force of the electrical sparks leads to an increase in the dielectric fluid flushing between the electrode (wire) and the workpiece. As a result, debris is removed vigorously and quickly from the plasma channel and the metal removal rate increases [22].

The surface roughness of the machined surface increases by increasing the spark energy and pulse of time. The electric spark energy impacts the machined surface and leads to more eroded material. When the thermal conductivity and the melting temperature of the material is low, the surface roughness is higher [23].

The machining of these alloy types encounters difficulties with the conventional processes as conventional processes may affect the alloy properties. Therefore, non-

conventional processes are the most suitable for these types of alloy. One of the most important and modern methods is the WEDM process, which is used in production lines to deal with conductive and semi-conductive materials to produce complex shapes [24].

The WireEDM machining process is controlled by a set of input parameters including pulse onTime Plus, Pulse off Time, and Servo voltage, which are the most significant input parameters. Some researchers have conducted studies to determine the effects of these input parameters on the machined surface in relation to surface topography, microstructure and micro-hardness [25-31].

WEDM currently is the dominant technology that is typical and suitable for precision conducting materials and cutting and complex forming processes. Undesirable effects on the machined surface, such as recast layers, cracks, heat-affected zones, and micro-voids, are considered to be lowest compared to other processes [32].

Improving machined surface integrity and quality is associated with the formulation of recast layers, cracks, oxides and carbide compounds on the machined surface. Reducing surface roughness can lead to improving fatigue life, corrosion and wear of the material [33].

Recently, studies have been carried out by Alidoosti, et al. [34]. who found that recast layers during the machining process lead to increasing machined surface hardness.

Discharge current and pulse time were found to be the most important input parameters affecting metal removal rate and surface roughness. Selecting the optimal parameters is one of the most important steps to reduce the cost of machining and improve the integrity of the surface to produce complex shapes [35].

Fan, et al. [36] has developed a micro-controller that adjusts WEDM input parameters. They found that the optimal pulse interval and pulse duration with a suitable capacitance selection leads to the best achievable surface finish.

Very limited studies focused on changes in hardness [37] and on the surface quality of the machined surface of the Nitinol alloy [6, 38].

Therefore, there is an urgent need to conduct more investigations into WEDM and μ-WEDM to study the effects of input parameters on the surface integrity of Nitinol alloys and to determine the relationship between the input and output parameters of the WEDM and μ-WEDM processes.

In this thesis, investigations were performed to observe the effects of μ-WEDM input parameters on Nitinol alloy. Adjustable input parameters were selected, such as peak current, servo voltage, pulse on time and pulse of time, and output parameters of the machined surface were studied, including metal removal rate "MRR", Kerf variation, white layer thickness, surface roughness and μ-hardness. Moreover, the effect of μ-WEDM machining parameters exerted on the Nitinol machined surface parameters was determined by performing an Analysis of Variance (ANOVA) based on the response surface methodology separately and simultaneously to achieve maximum MRR and minimum white layer thickness, surface roughness, kerf variation, and μ-hardness.

1.3 Scope of the Thesis

Chapter 1 presents the introduction, literature view and the aim of the work.
Chapter 2, Experimental Setup and Methodology, presents the research motivations, research approach, and methodology.

In the methodology section, the specification of the Nitinol alloy and μ-WEDM cutting machine, Nitinol alloy samples treatment processing and test preparations are performed. Measurements of Kerf width variation were then made and the metal removal rate MRR was calculated. The thickness of the white layer was measured using SEM and their compositions were analyzed using an EDX unit. The machined surface composition was measured using an EDX unit and the arithmetic surface roughness of the machined surfaces of Nitinol samples was measured using a laser confocal microscope. Surface roughness images were analyzed using AFM software based on ISO 25178. The μ-hardness of the machined surface was measured using the Vickers scale and compared with the μ-hardness of the bulk material in order to recognize the μ-hardness changing in the white layers due to the application of different μ-WEDM cutting parameter conditions.

Chapter 3, Design of the Experiments and Results Analyses, presents the experiment design, surface response methodology, optimization analysis approaches, Analysis of Variance (ANOVA) and Optimizations.

In this section, the experiment tests are designed according to the orthogonal Taguchi array L27. A regression analysis (ANOVA) was performed for each of the machined

surface output parameters of the Nitinol sample separately. ANOVA was also performed according to the response surface methodology (RSM) to determine which dominant input parameters would affect the machined surface parameters (kerf variation, white layer thickness, metal removal rate, surface roughness, and μ-hardness). The regression model was then extracted for each output parameter separately, and then an optimization analysis was performed to obtain the optimal value of the output parameter at the best input parameter set. In addition, an optimal analysis of the combined output parameters was carried out simultaneously to determine the optimal value for each and the best μ-WEDM cutting parameters were set according to this.

Chapter 4 presents the findings and conclusions of this thesis. Possible future works in this field are also described.

CHAPTER 2

Experiments Setup and Methodology

2.1 Research Motivations

Our motivations for this thesis were to study and investigate the effects of cutting parameters in the μ-WEDM process on Nitinol alloy to achieve optimum cutting parameters with fewer undesirable effects on the machined surface of the Nitinol alloy.

2.2 Approach

The literature review was presented in the first chapter according to the previous works of other researchers on the effect of cutting parameters on the machined surface of the Nitinol alloy.

In this thesis, the sample was prepared with dimensions of 5 mm × 10 mm × 100 mm using water jet technology.

Nine kerfs were conducted according to a particular design in which a variety of cutting parameters was selected on the μ-WEDM machine.

Grinding, polishing and etching processes were carried out and cleaning was performed using distilled water and acetone liquid using an ultrasonic device to obtain the best results. Other measurements, including metal removed rate, kerfs width, white layer thickness, surface roughness and microhardness, were made later to determine the effects of the μ-WEDM parameters on the machined surface of the Nitinol alloy sample.

2.3 Methodology

2.3.1 Material Specifications

In this study, a sample with dimensions 60 mm × 10 mm × 5 mm was prepared for the experiments and 9 kerfs were used with different cutting parameters (see Figure 2.1).

Table 2 1 Nitinol alloy specifications

Melting point	1300 ^{o}C
Density	6.45 g/cm^{3}
Specific heat	0.20 cal/g^{o}C
Af temperature	20±5^{o}C
Standard	ASTM F 2603

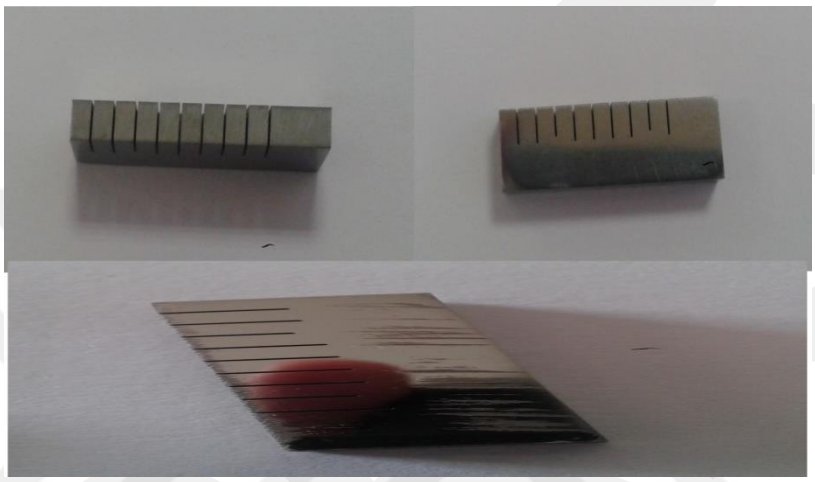

Figure 2. 1 Nitinol alloy “used sample”

2.3.2 µ-WEDM Machines specifications:

A high precision WEDM (Sodick AP250L, Micro Manufacturing Laboratory, Bilkent University) was implemented to perform the experiments. Figure 2.2 shows the machine that was used as well as the relative position of the tool wire and workpiece manipulation. A 100 µm diameter brass wire was used as the tool and HEC(O) oil as the dielectric liquid.

Figure 2. 2 μ-WEDM (Sodick AP250L) used to conduct the experiments on the Nitinol alloy sample

Four parameters, namely pulse on time, pulse off time, servo voltage and peak current were identified. The range of each parameter was determined from the preliminary experiments. Each process parameter was investigated at three levels to study the non-linearity effect of the parameters. The identified controllable parameters in the μ-WEDM of the TiNi SMA experiments and their levels are listed in Table 2.2, which shows the machining parameters, which are fixed throughout the investigation.

Table 2 2 adjustable parameters and their levels

Code	Parameters	Level 1	Level 2	Level 3
Ip	Peak current	3	10	15
T_{on}	Pulse on time	0	1	2
T_{off}	Pulse of time	3	10	15
Sv	Servo voltage	80	130	180

Table 2 3 Fixed parameters and their values

Code	Parameter	Value
HRP	Auxiliary power supply circuit	213
MAO	Pulse duration	790
V	Main power supply voltage	1
C	Capacitor	2

WT	Tension control	30
WS	Wire speed	46
	Flushing pressure	3 L/min

The brass wire of 0.1 mm in diameter was selected as electrode, and oil [HEC (O)] is chosen as dielectric liquid with flushing pressure 3 L/min, as shown in Figure 2.3.

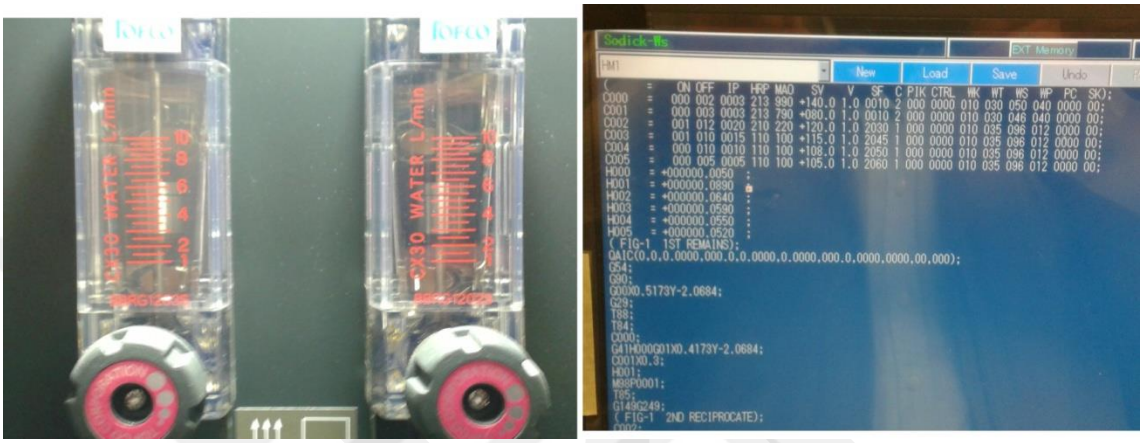

Figure 2. 3 Flushing dielectric liquid and fixed parameters values

2.3.3 Grinding, Polishing, and Etching

Grinding was performed on the sample with silicon carbide (SiC) 800-grade, 1000-grade, and 2500-grade paper. Polishing was performed using two suspension liquids, namely aluminum dioxide (AI_20_3) 1 µ, and diamond 0.3 µ suspensions. Ultrasonic cleaning was performed for 10 minutes using acetone and distilled water after every step. For clear images on the SEM, it was necessary to apply an etching process on a cross-section of the machined surface of the sample. One example of a useful etching solution for Nitinol alloy, which is composed of 10 ml HF, 20 ml HNO_3 and 30 ml HO_2 [39], was used as an etching solution applied for 2 seconds. In the final step, alcohol was used to wash the sample. After the grinding, polishing and etching processes, the machined surface of the sample was checked using a Nikon LV150 microscope. Figure 2.4. and Figure2.5 shows the grinding, polishing, cleaning and etching tools.

Figure 2. 4 Nikon LV150 microscopy

Figure 2. 5 Grinding, polishing, cleaning, and etching processes

2.3.4 Kerfs and Metal Removed Rate "M.R.R" Measuring

The accuracy of the workpiece during the µ-WEDM processes is measured by measuring the kerf width. The µ-WEDM processes are mainly based on cutting using a high density of electrical discharge pulses with a very high temperature of up to 12,000°C. Pressurized flushing liquid was used to clean any eroded particles and to separate between the "anode" workpiece and the cathode "wire." These factors have direct effects on wire vibration and result in less precision in the dimensions of the workpiece. Figure 2.6 shows the kerf width during the µ-WEDM process.

The metal removal rate is an important factor that affects production capacity and quality in factories. The metal removal rate can be defined as the amount of metal removed from a workpiece within a specified time, usually within a minute. The metal removed rate (MRR) as a function of the Kerf width, the workpiece thickness and the

feed rate can be calculated in cubic millimeters per minute or milligram per minute (mm^3/min, or mg/min), as shown in Eq. 2.1. An average of at least 20 readings of the feed rate values for a 4 mm cutting length was calculated for each Kerf.

$$MRR = Kerf\ width * workpice\ thickness * feed\ rate \quad \textbf{(2.1)}$$

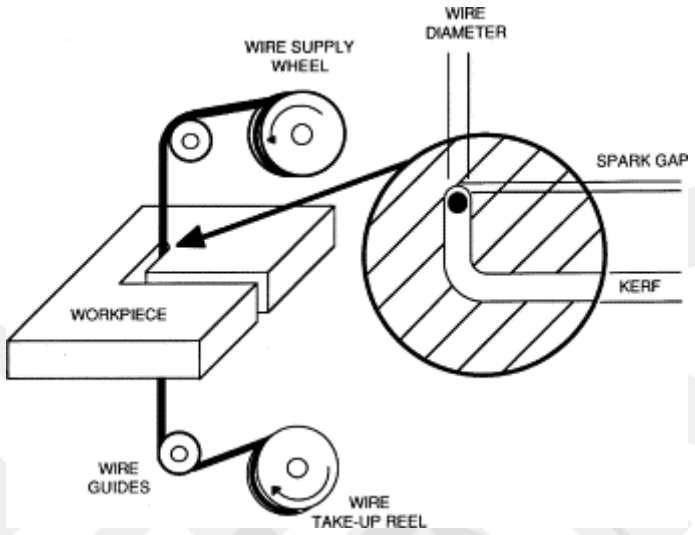

Figure 2. 6 Photographic to the view of the kerf width [40].

The scan electron microscope (SEM) EVO LS15 (MFCE, Atilim University, Figure 2.7) was used to measure the kerf width. SEM images at 500× magnification of the kerfs from 1 to 9 for three different places with different cutting condition parameters are shown in Figures 2.8 to 2.12 below.

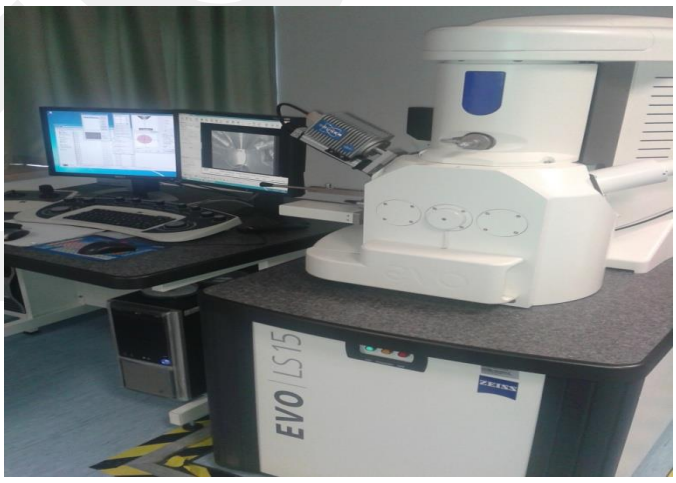

Figure 2. 7 Scan Electron Microscopy EVOLS15

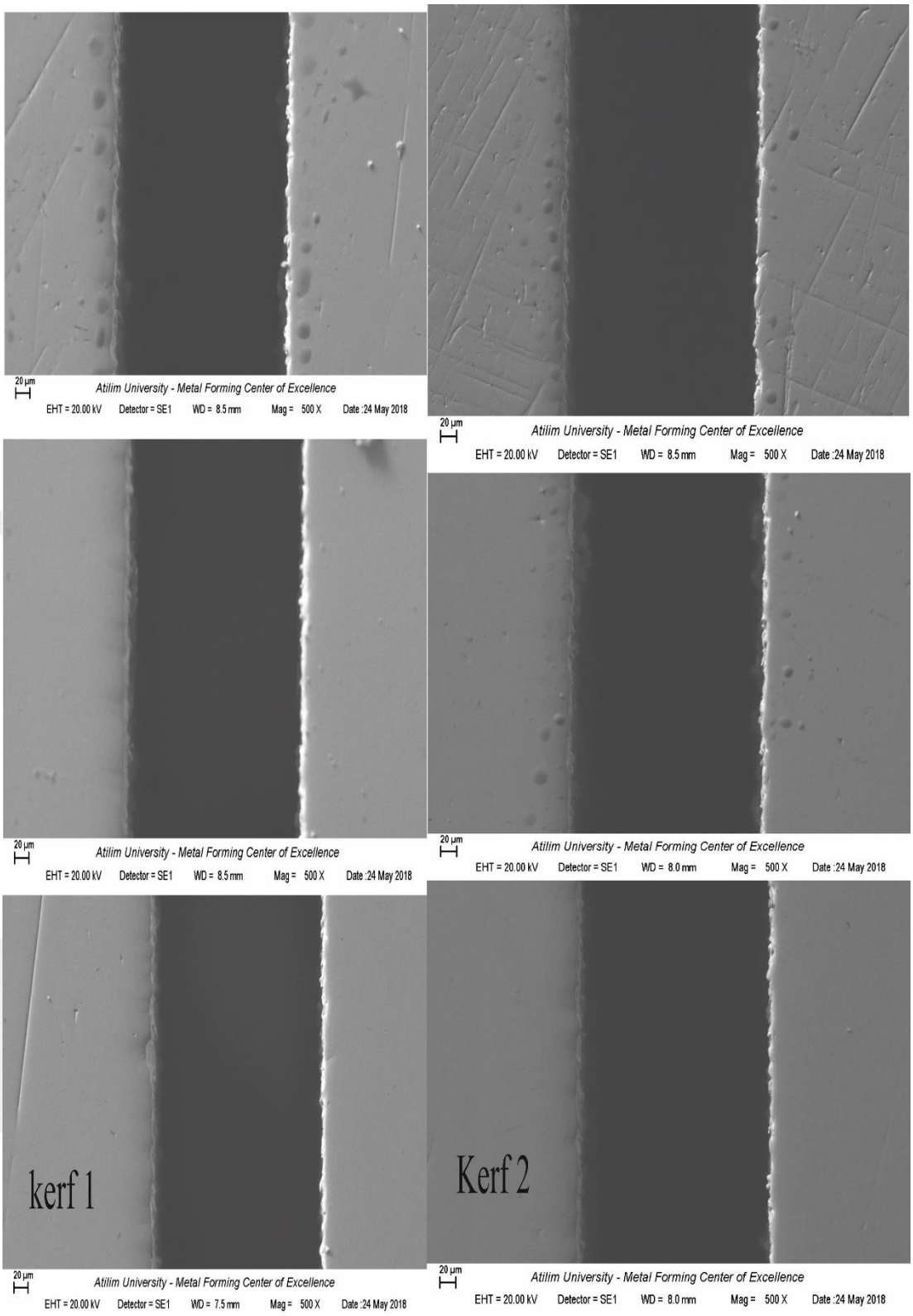

Figure 2. 8 SEM micrograph of firest and second Kerf at 500x magnification

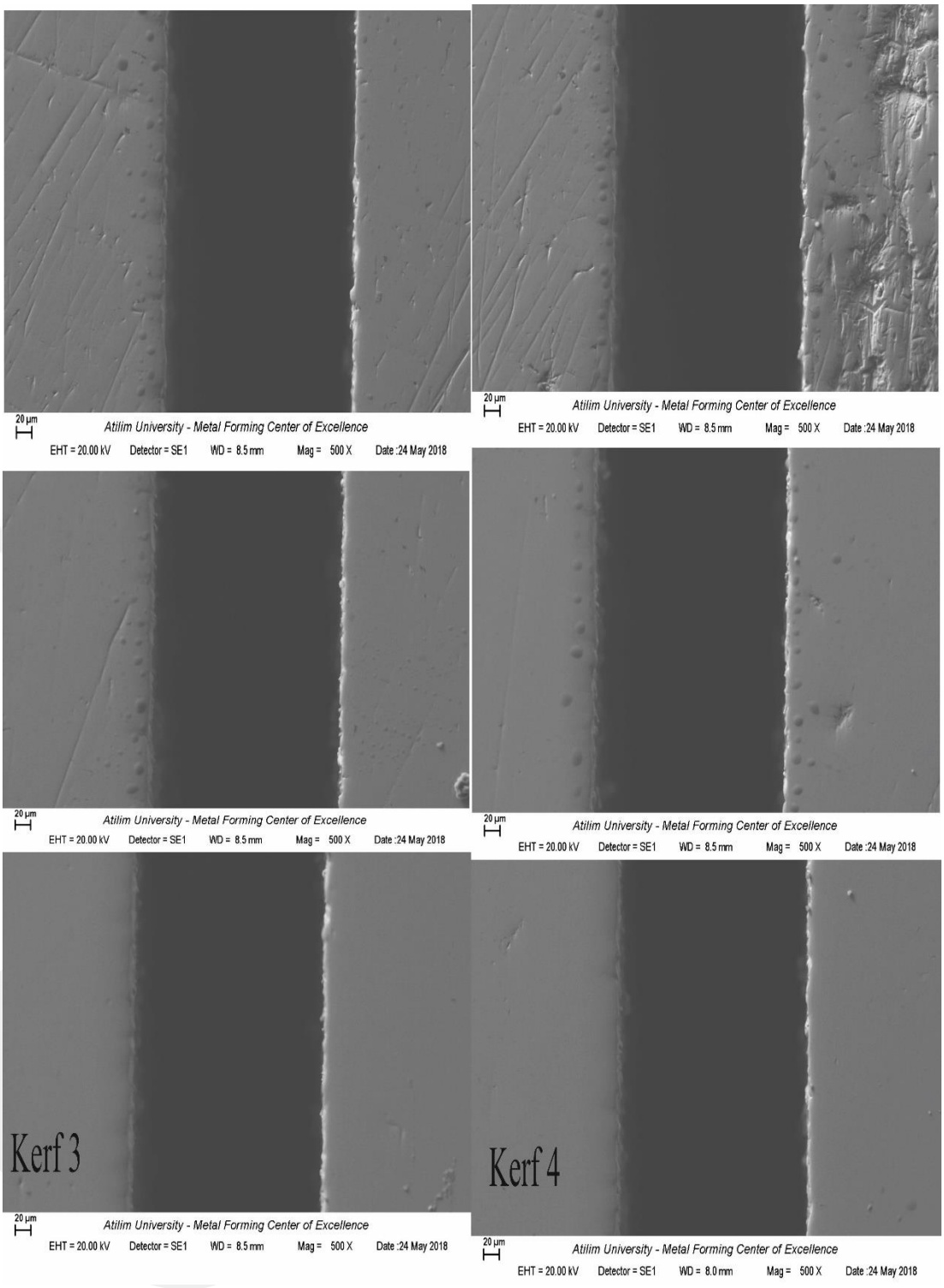

Figure 2. 9 SEM micrograph of third and fourth Kerf at 500x magnification

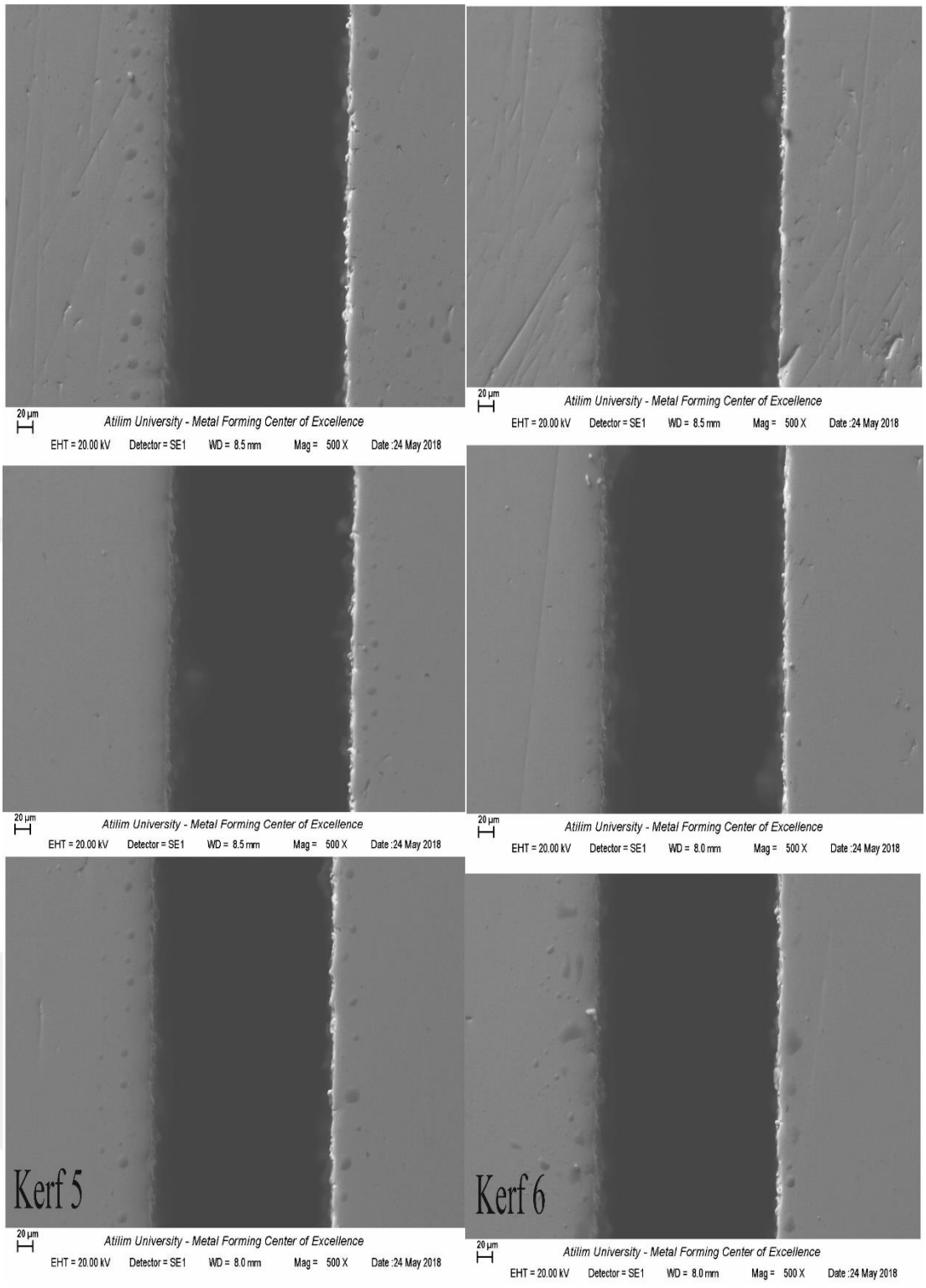

Figure 2. 10 SEM micrograph of fifth and sixth Kerf at 500x magnification

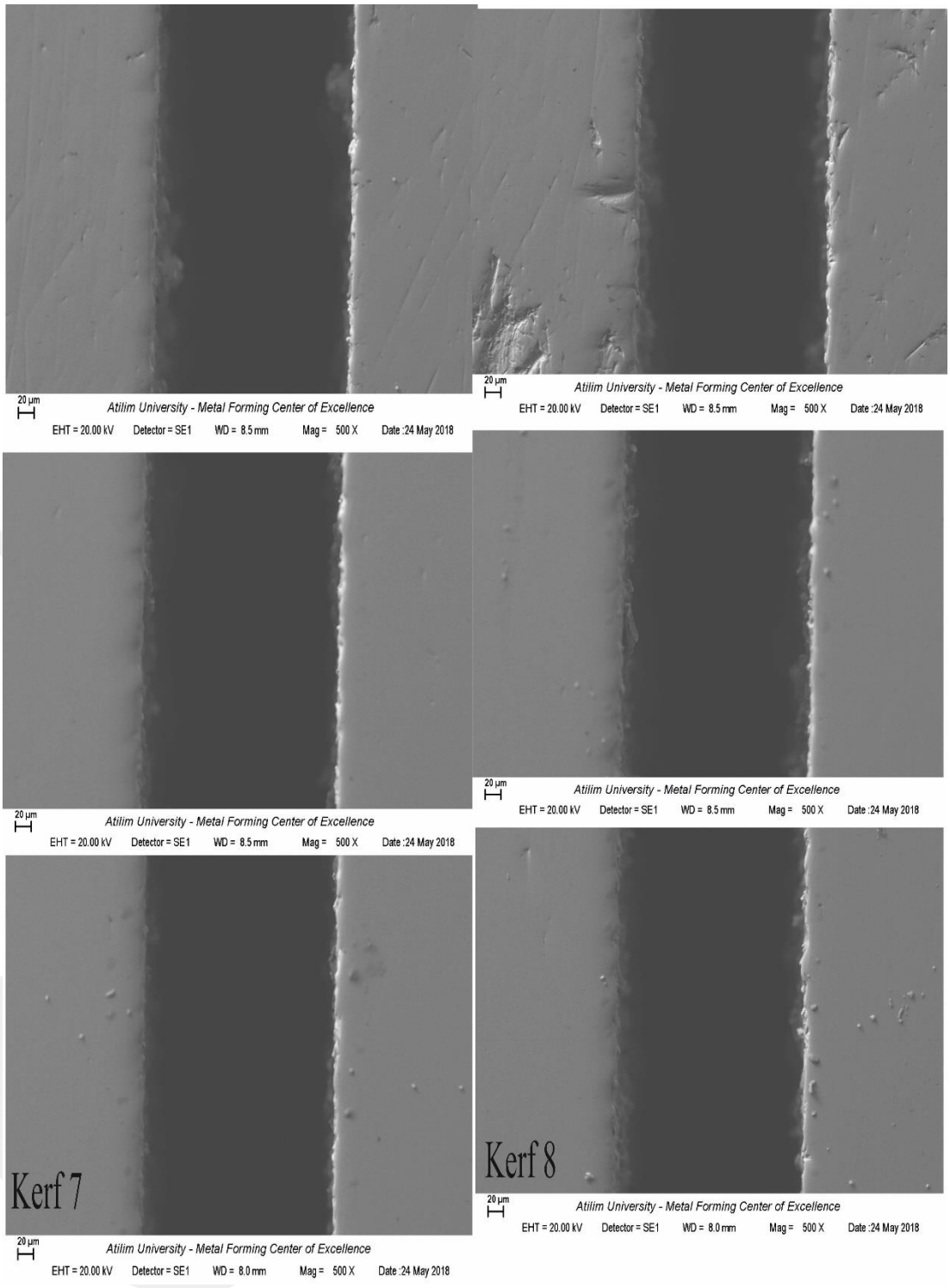

Figure 2. 11 SEM micrograph of seventh and eighth Kerf at 500x magnification

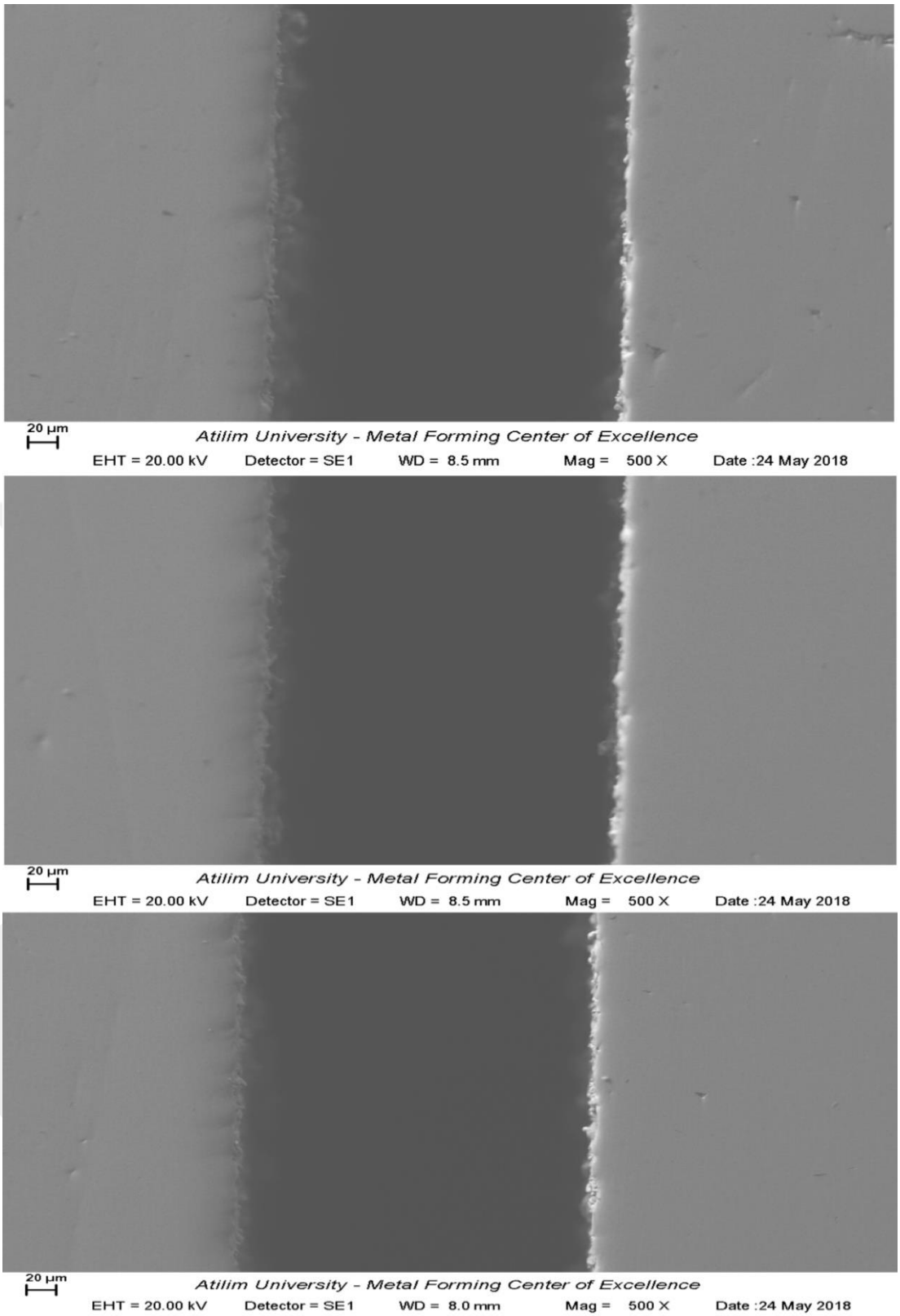

Figure 2. 12 SEM micrograph of ninth Kerf at 500x magnification

2.3.5 White Layer Thickness (W.L.T.) Measuring

During the cutting process using the μ-WEDM, the workpiece is exposed to a high temperature of up to 12,000°C [39] because of the high energy of the electric sparks generated between the cutting wire and the workpiece surface during the cutting process. Since the temperature of the dielectric fluid is low relative to the debris, part of the debris re-solidifies on the machined surface of the workpiece and another part is removed due to the flushing pressure.

This debris accumulates and precipitates on the surface of the workpiece causing what is known as a recast layer, whose mechanical and physical properties are quite different from the Nitinol alloy and do not have the same significant properties of the Nitinol alloy, especially the shape memory effect (SME) and pseudoelasticity.

The debris deposited on the machined surface consists of several different phases with different compositions and properties, which is eroded from the brass wire and the nickel and titanium is dissolved from the Nitinol alloy. Because of the very high temperature, these elements combine with other elements, such as carbon and oxygen, forming carbides and oxides on the machined surface. They may fuse together into a new crystalline system such as Ni or Ti rich phases forming another compound with properties different from Nitinol alloy. These phases are responsible for the increase in the hardness and roughness of the machined surface.

In order to know how to control the thickness of the white recast layers and how they are formed, it is necessary to conduct experiments with various different μ-WEDM parameters and make measurements of the white recast layer thickness formed on machined surface using a scanning electron microscopy (SEM) device equipped with an energy dispersive X-ray spectrometry (EDS) unit to study the thickness of the white recast layers and its compositions to improve machined surface integrity of the Nitinol alloy sample. Figure 2.13 shows SEM quanta 200f (Micro System Design and Manufacturing Center, Bilkent University) with the EDS unit that was used to scan the recast layer and conduct an EDS analysis of its composition.

Figure 2. 13 SEM quanta 200f with EDS unit used to scan the white recast layer

Figures 2.14 to 2.18 show SEM images of 9 kerfs measured at two different places for every kerf with their EDS analyses.

The EDS spot analysis was performed on the highest thickness of the white layer that can be seen on the cross-section of each Kerf. It is clear that the most concentrated constituent elements are the titanium and nickel-rich phases, which resulted from the decomposition and melting of the Nitinol alloy during the μ-WEDM process and re-solidification on the machined surface of the workpiece. This apparent composition can be clearly observed in the EDS analyses for every kerf (Figures 2.14 to 2.18).

In addition, some other phases deposited on the surface of the white layers can be observed in small quantities when compared to the nickel and titanium-rich phases. For example, the carbon element can be seen in the 6^{th} and 7^{th} kerfs (Figures 2.16 and 2.17) and the elements of carbon and aluminum in the 2^{nd} Kerfs (Figure 2.14. We note the presence of oxygen and aluminum in the 4^{th} and 5^{th} kerfs (Figures 2.15 and 2.16). The main cause of the presence of aluminum and carbon may be the residue of some residual particles from the polishing process as a result of the use of aluminum dioxide and diamond suspension liquids.

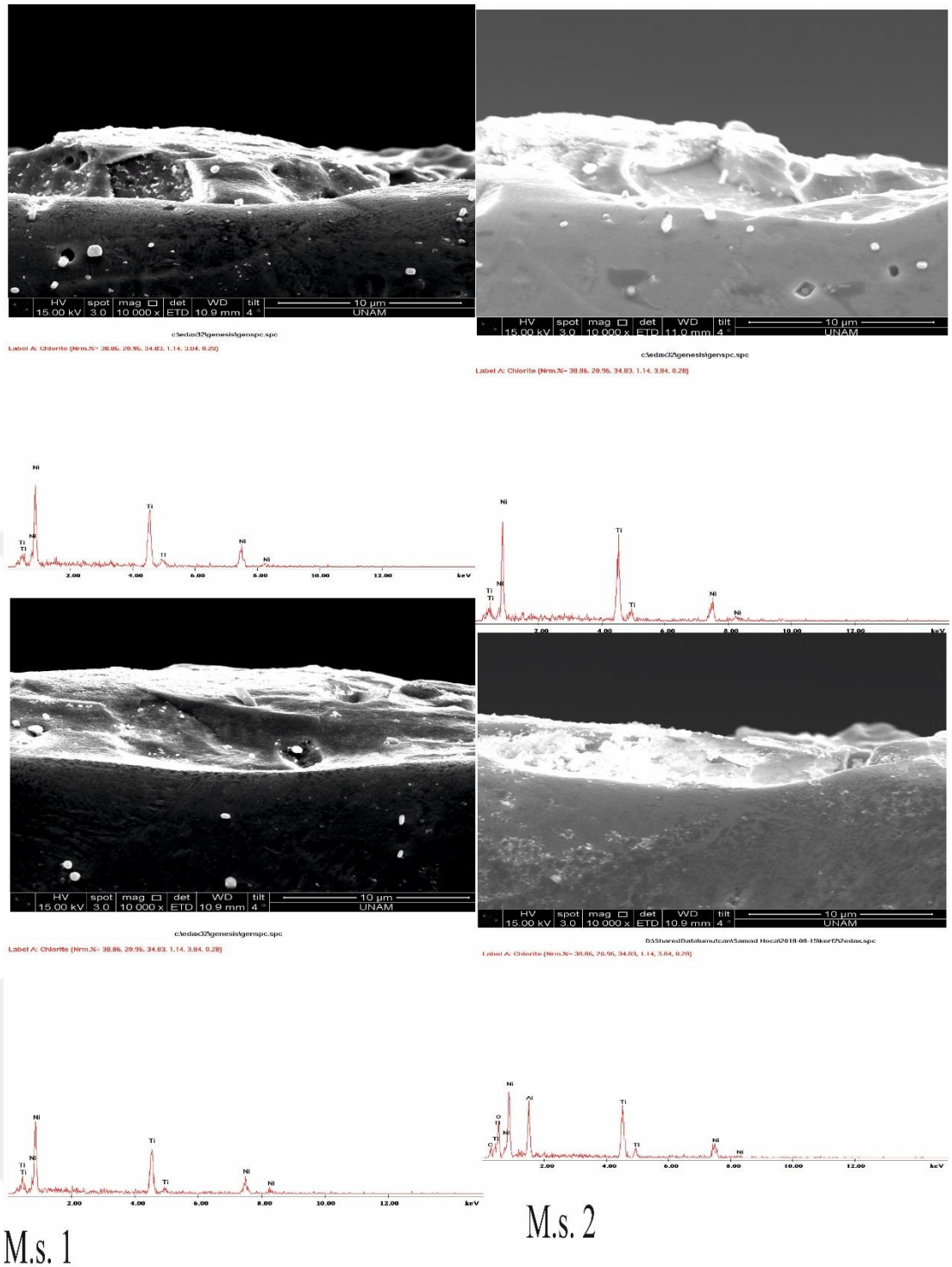

Figure 2. 14 SEM white layers images of firest and second kerfs measured at two different places with their EDS analysis.

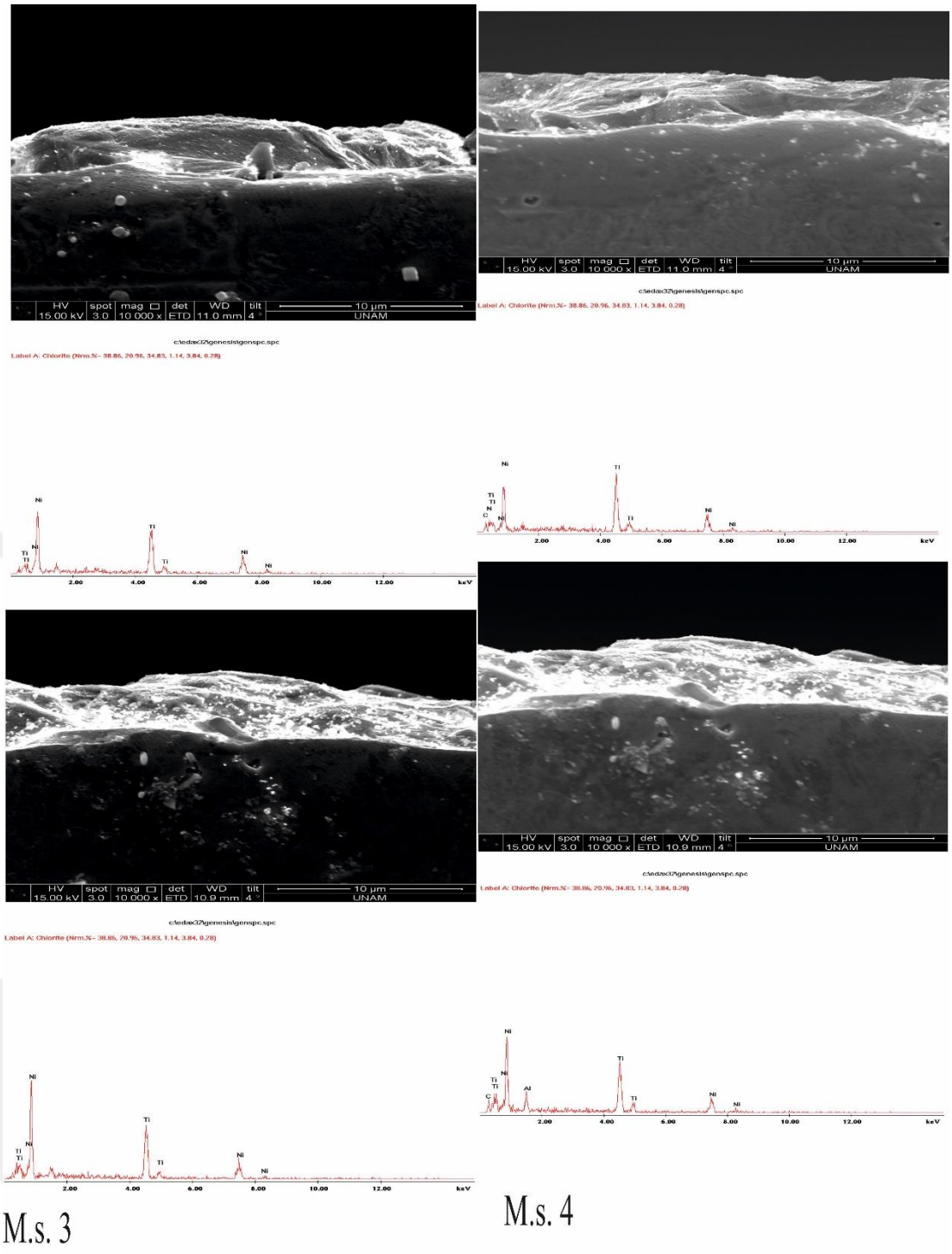

Figure 2. 15 SEM white layers images of third and forth kerfs measured at two different places with their EDS analysis

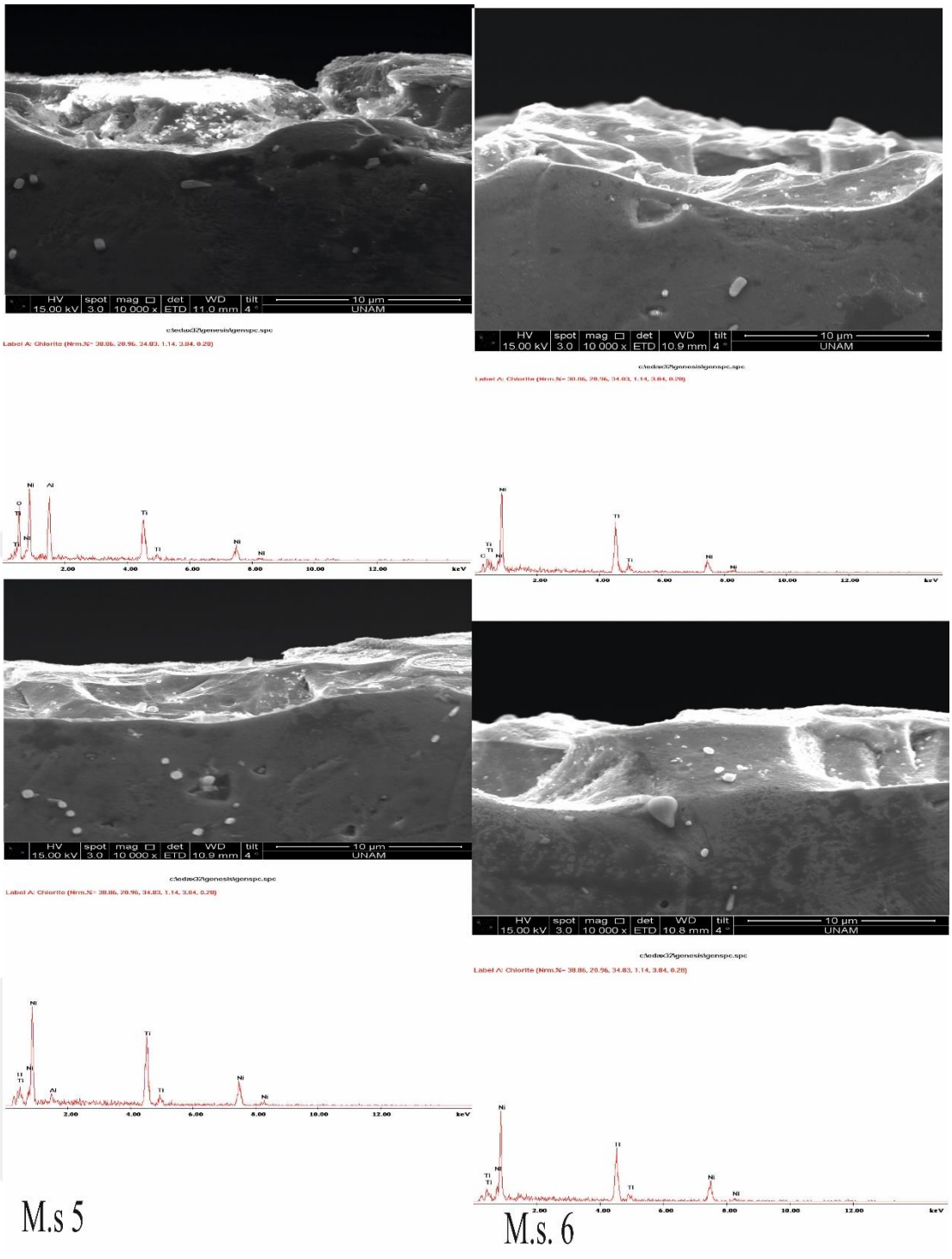

Figure 2. 16 SEM white layers images of fifth and sixth kerfs measured at two different places with their EDS analysis

.

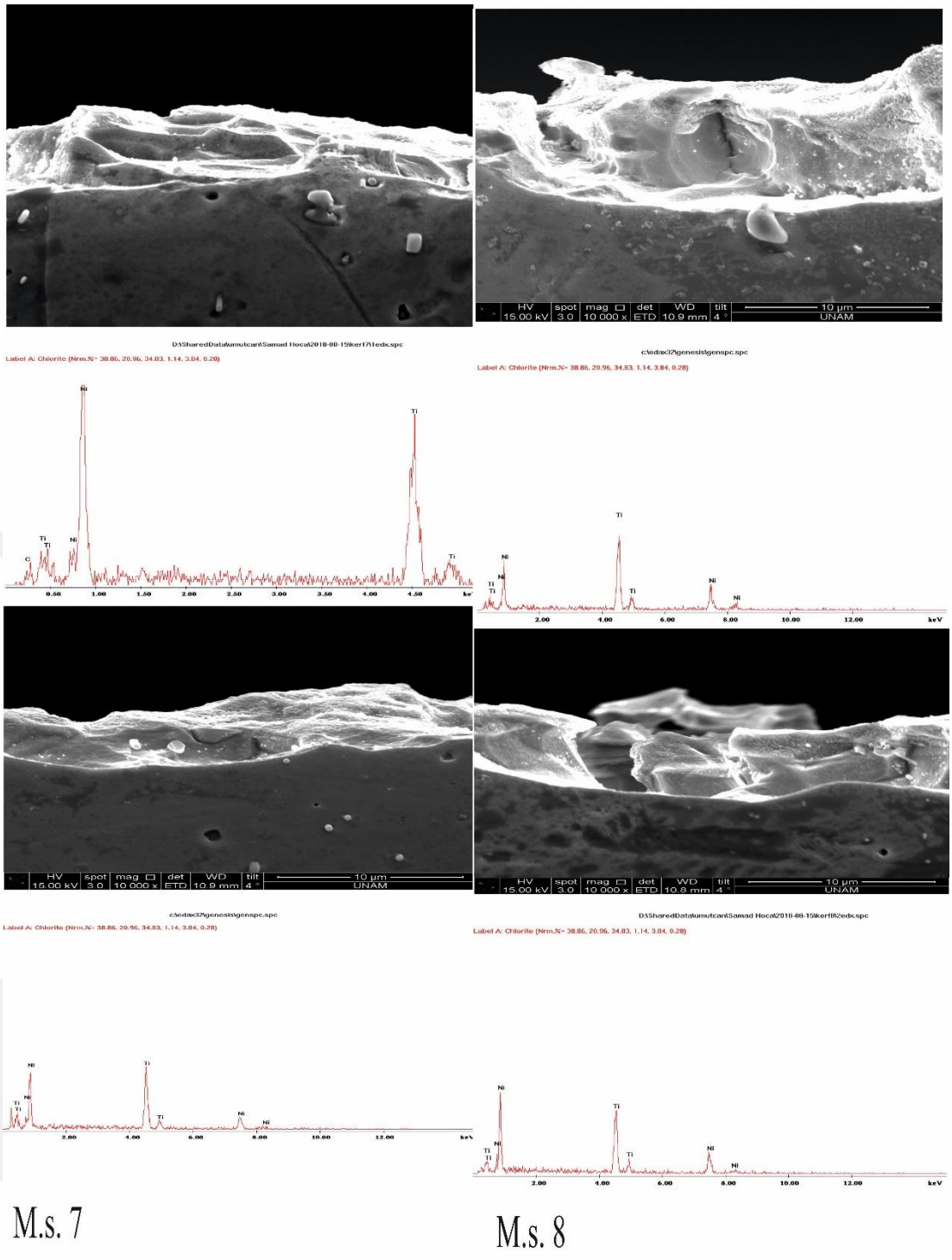

Figure 2. 17 SEM white layers images of seventh and eighth kerfs measured at two different places with their EDS analysis

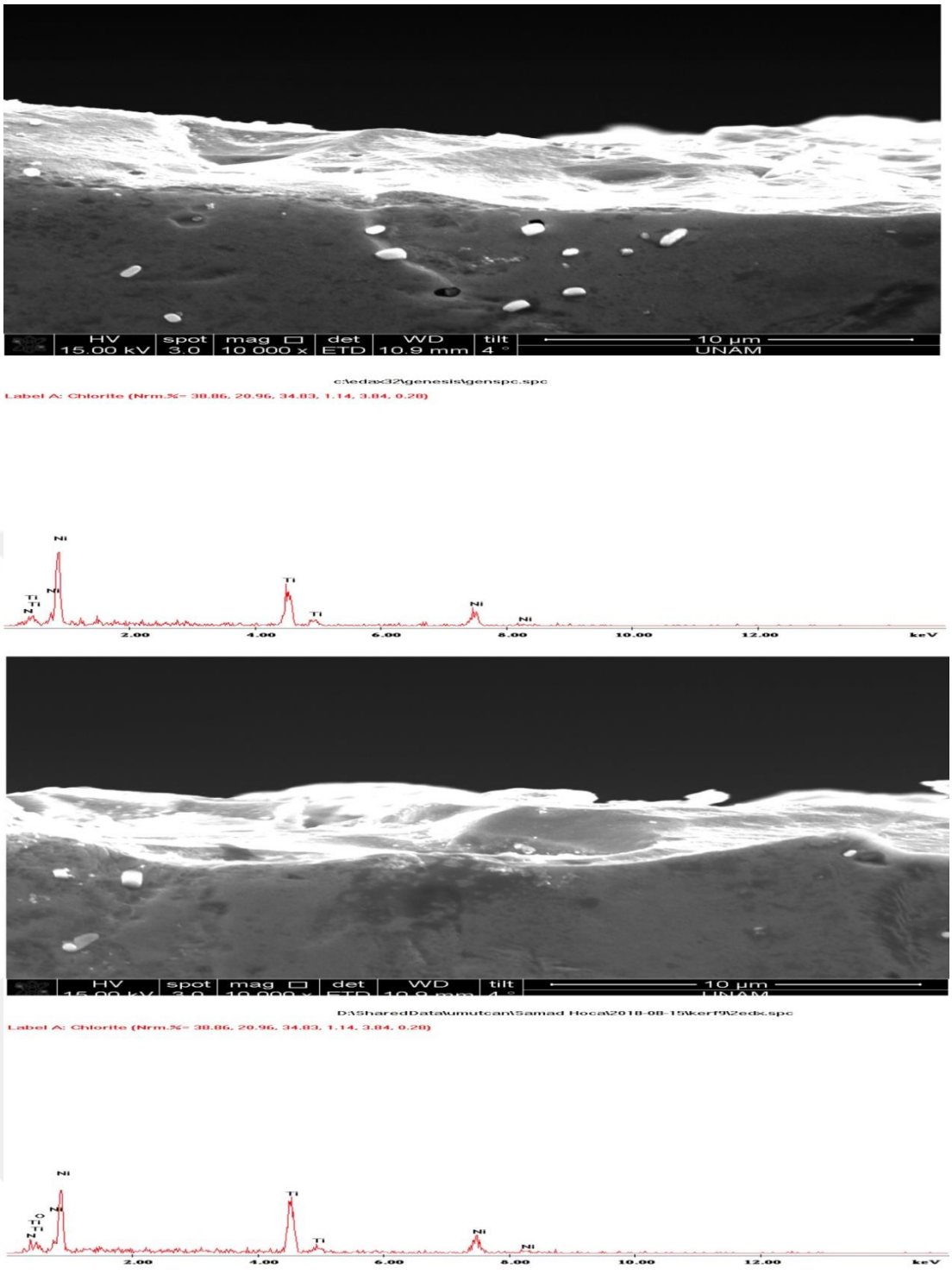

Figure 2. 18 SEM white layers images of ninth kerfs measured at two different places with their EDS analysis

.

2.3.6 Topography Characterization and Mechanical Properties Tests

Nine Nitinol samples were separated from the main sample (Figure 2.1) using a milling machine based on the number of kerfs being used using the μ-WEDM (Sodick AP250L) machine. A Microstructure of Surface morphology study was performed using EDS to check any new phases forming on the machined surface. Surface roughness tests were conducted to check the surface integrity of the machined surfaces of the nine samples, all of which were then fixed to the aluminum plate (Figure 2.19) in order to conduct micro-hardness tests.

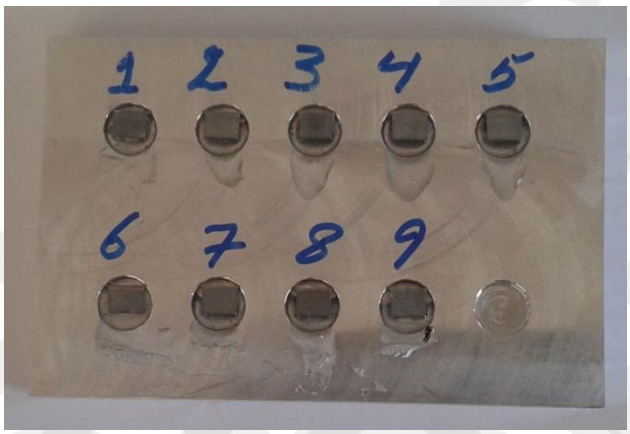

Figure 2. 19 The nine samples on the aluminum fixture

2.3.6.1 EDS Analysis of Microstructure

The SEM quanta 200f with an EDS unit (Micro System Design and Manufacturing Center, Bilkent University; Figure 2.13) was used to scan the machined surface of every sample and conduct EDS analyses of their compositions. Magnification factors of 350× and 4,500× were applied to study the machined surface4,500 and analyze the components using the EDS unit to study the surface morphology and recognize different phases forming on it.

Figures 2.20 to 2.24 show SEM images and EDS analyses of nine machined surfaces with different cutting μ-WEDM parameters.

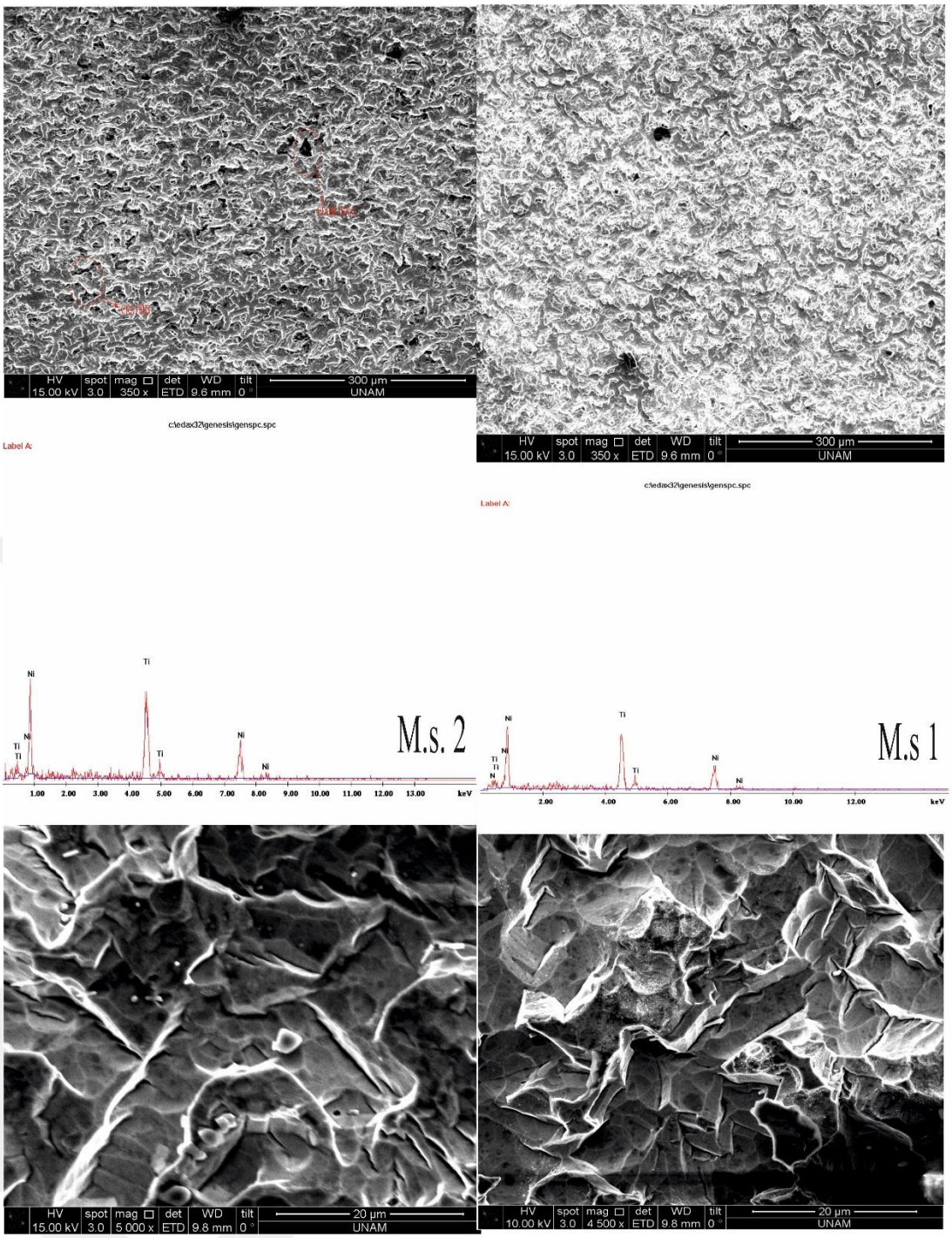

Figure 2. 20 SEM image at 350× and 4,500× magnification factors and EDS analyses of the first and second machined surface samples

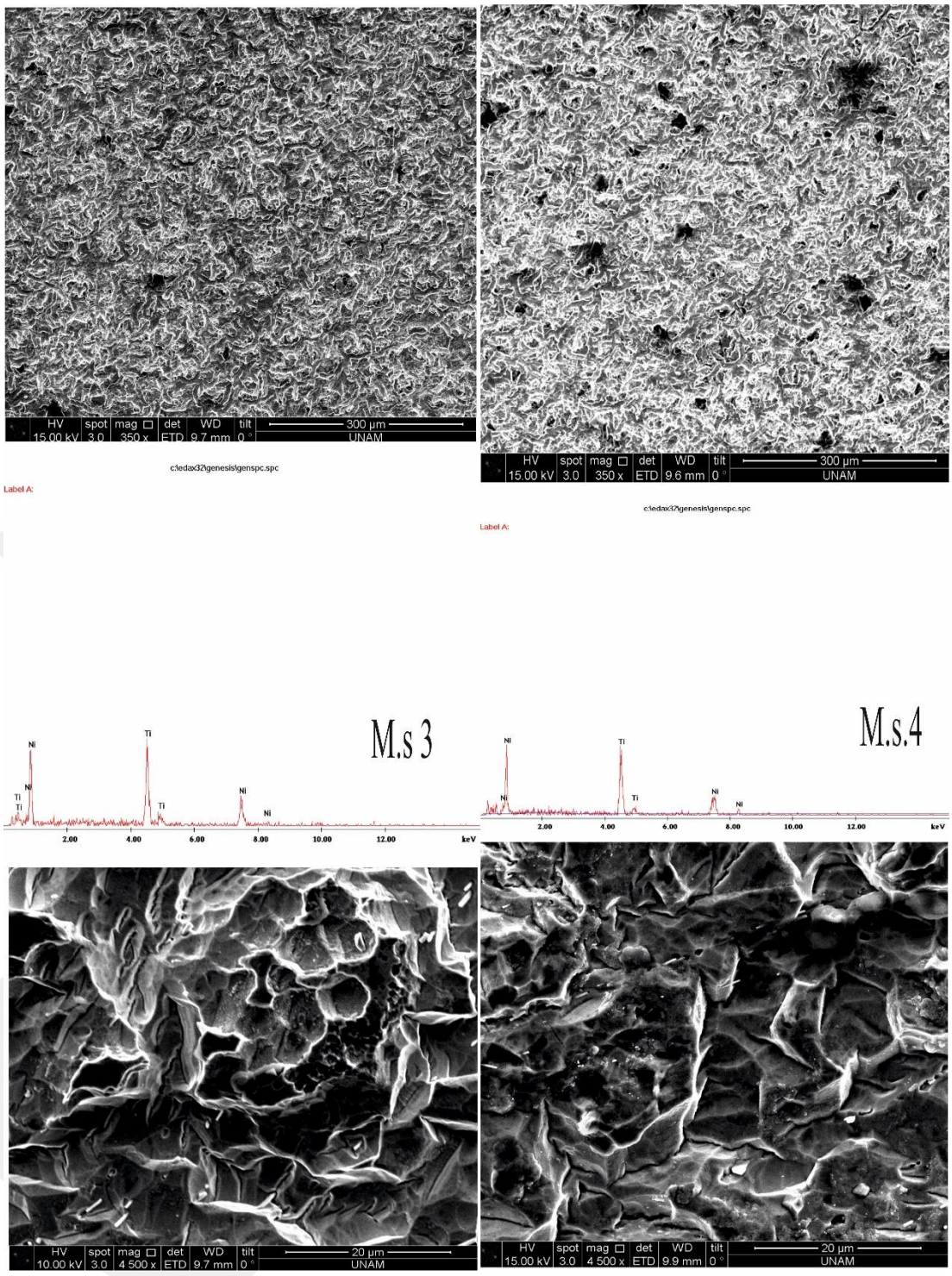

Figure 2. 21 SEM image at 350× and 4,500× magnification factors 4,500and EDS analyses of the third and fourth machined surface samples

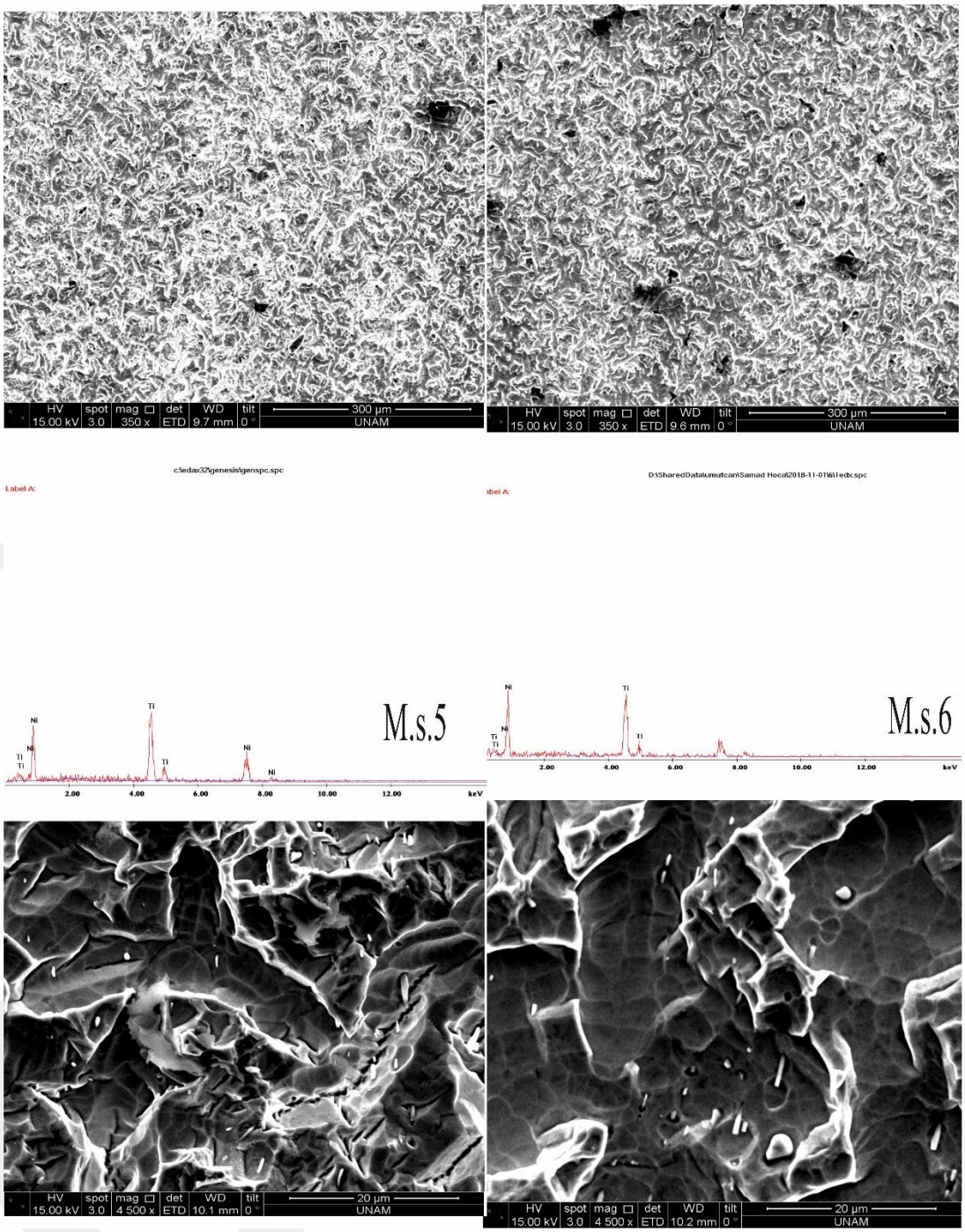

Figure 2. 22 SEM image at 350× and 4,500× magnification factors and EDS analyses of the fifth and sixth machined surface samples

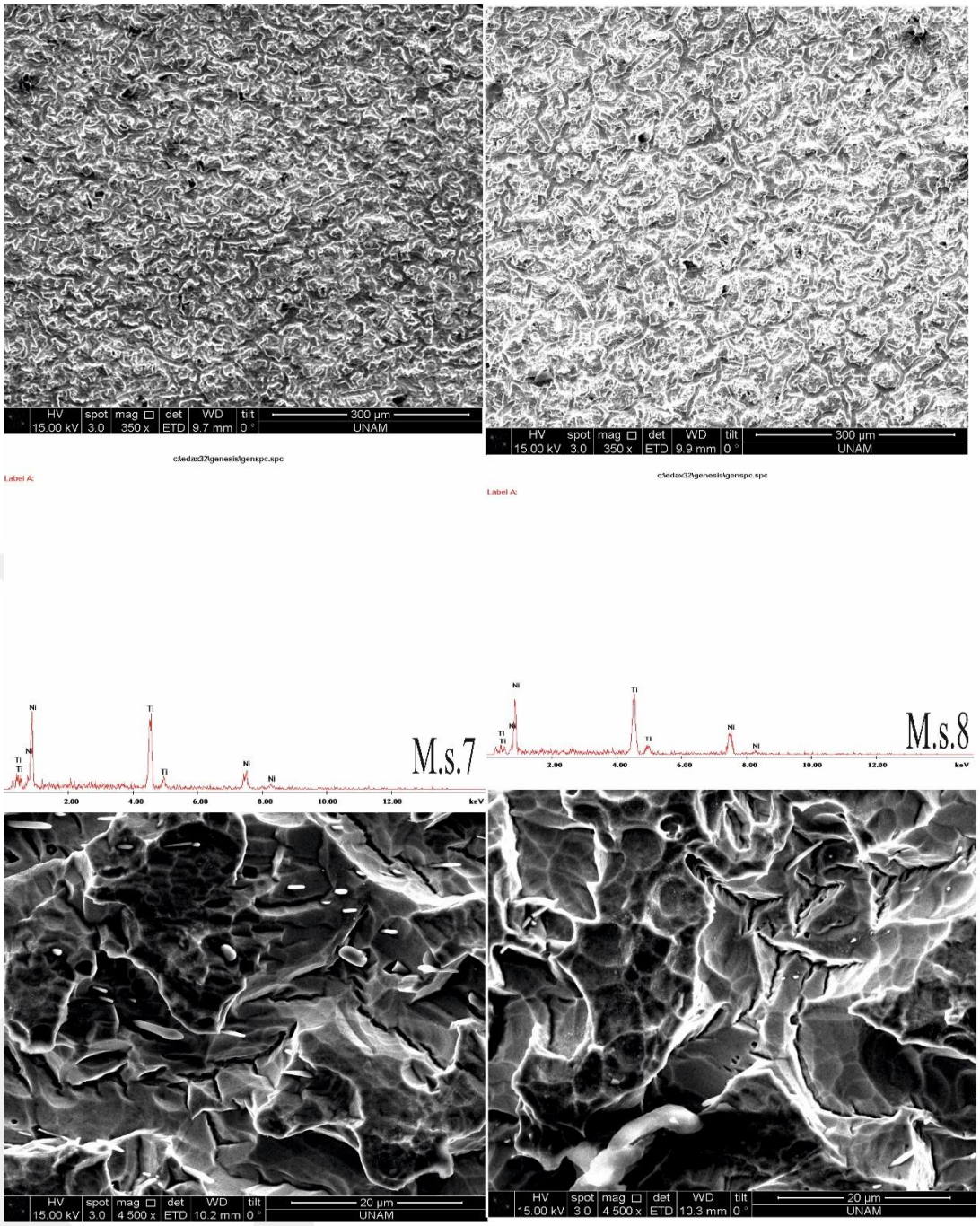

Figure 2. 23 SEM image with two magnification factors x350, x4500, and EDS analysis of seventh and eighth machined surface's sample

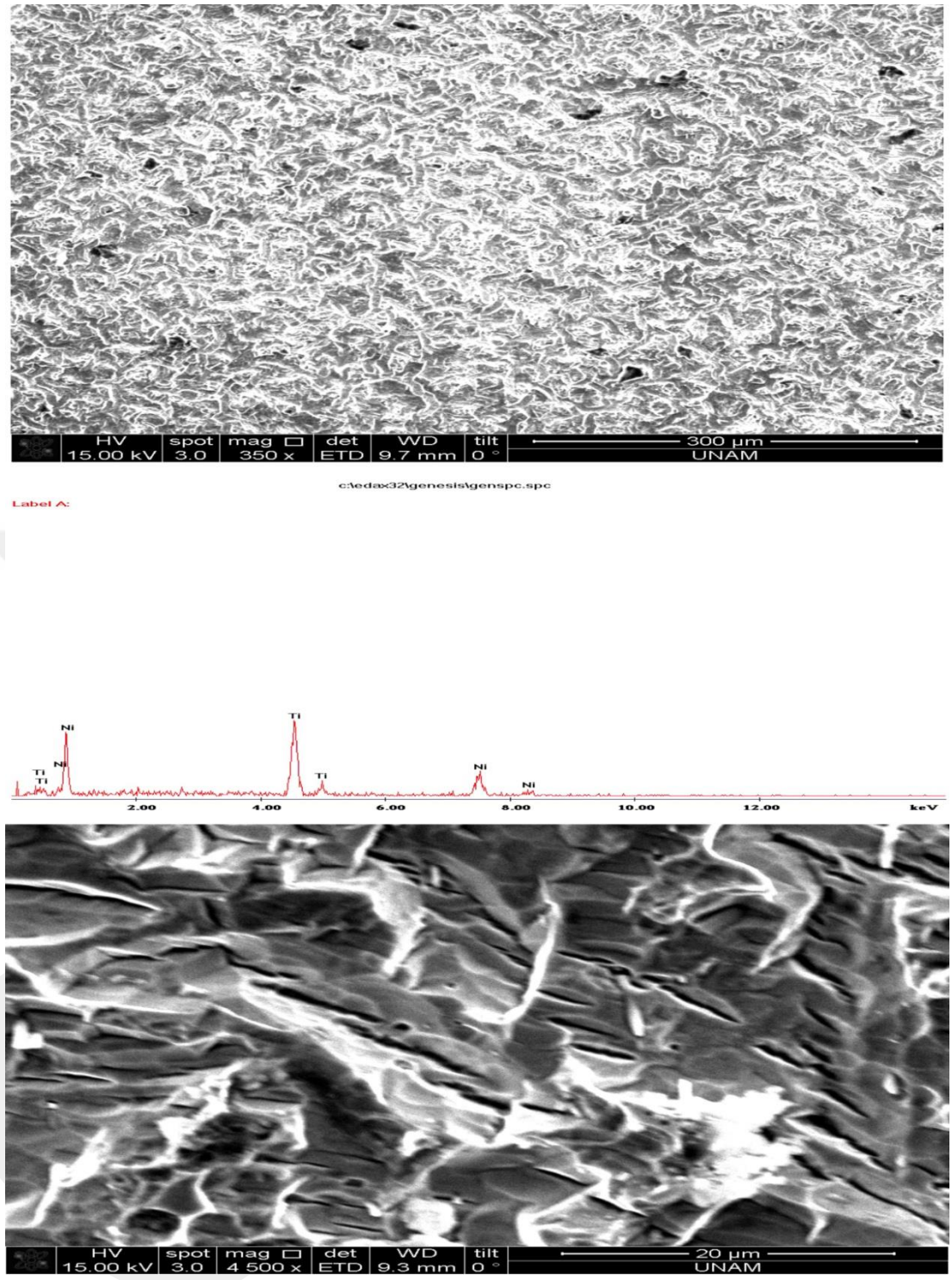

Figure 2. 24 SEM image at 350× and 4,500× magnification factors and EDS analyses of the ninth machined surface sample

Figures 2.20 to 2.24 show that the analyses of the machined surface phases components are almost equal, which are phases rich in nickel and titanium elements. With the exception of Figure 2.20, the presence of nitrogen can be seen within the

components. This may be due to the presence of one of the nitric acid compounds having reacted during the etching process.

The SEM images at 350× magnification view the craters and blowholes and at 4,500× magnification view the micro-cracks on the machined surfaces. These images show that the machined surface mostly containing a blowhole is seen in the 1st, 4th and 6th figures (2.20, 2.21 and 2.22). The 1st, 4th and 9th surfaces have the highest number of craters and micro-cracks (Figures 2.20, 2.21 and 2.24). In addition, it can be seen that the 6th surface is the lowest among the other surfaces in terms of the number of micro-cracks (Figure 2.22).

2.3.6.2 Surface Roughness (Sa) Measuring

Surface roughness is one of the most important output parameters affecting the quality of the machined surface. There are a couple of µ-WEDM input parameters that have a significant effect on surface roughness. These parameters include electrical and non-electrical parameters. However, the electrical factors have the greatest direct impact on the quality of surface roughness of machined surfaces.

Due to the high density of electric sparks during the time of cutting, craters, micro-cracks and blowholes are usually formed on the machined surface. The surface roughnesses were measured using a precise confocal laser scanning microscopy (KEYENCE Vk-x100 series, Micro Manufacturing Laboratory, Bilkent University) with a 50× magnification lens and a scanning rate of approximately 0.08 µm/s. Figure 2.25 shows the confocal laser microscopy KEYENCE vk-x100 series.

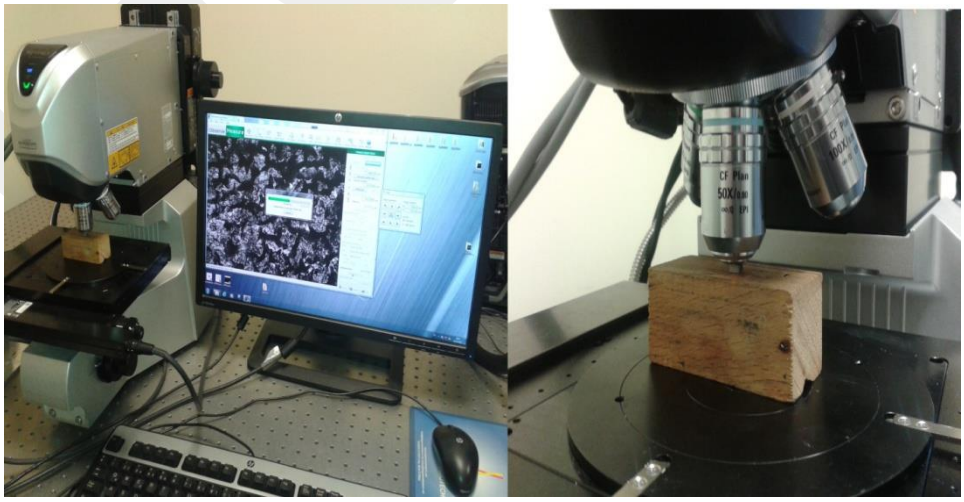

Figure 2. 25 Confocal laser microscopy KEYENCE Vk-x100 series.

The arithmetic mean surface roughness (R_a), which is commonly used in industrial fields, is measured in this work. The effect of the input parameters on the surface roughness of the machined surface was evaluated through the values of R_a based on ISO 25178.

An atomic force microscopy (AFM) program from www.profilmonline.com was used to analyze surface roughness images taken with a laser confocal microscope device. Through the analysis features in the program, area roughness features were applied. Additionally, some important filters were applied especially in the analysis method. The Gaussian method was used to obtain a complete unreduced image of the selected area with a cutoff length of 0.8 µm. The inclination filter was also applied to avoid analysis errors caused by the inclination of surfaces, especially since a wooden fixture was used. Figure 2.26 shows the AFM analysis program.

The surface roughness measured at three different points on each machined surface and photographs from Figures 2.27 to 2.31 show the surface roughness measured for all of them.

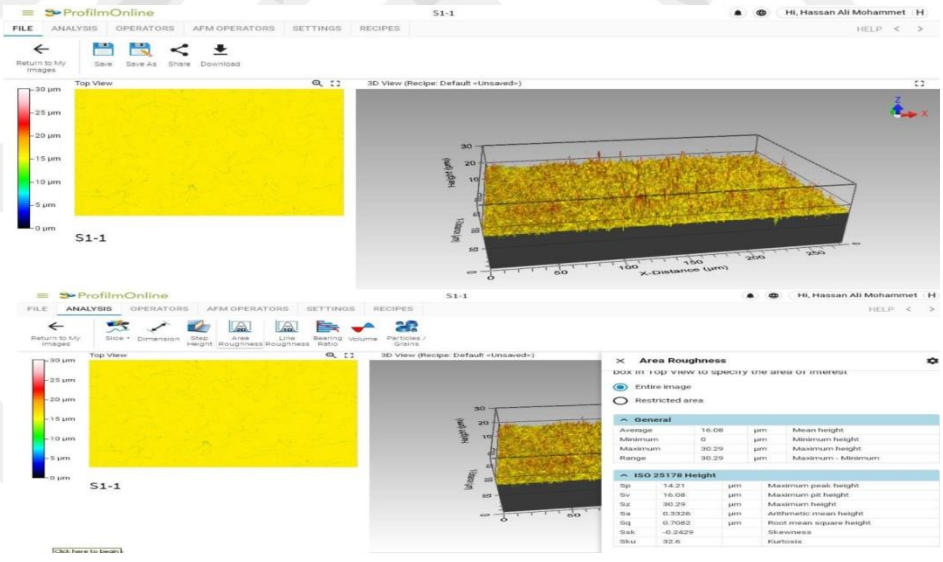

Figure 2. 26 AFM analysis program

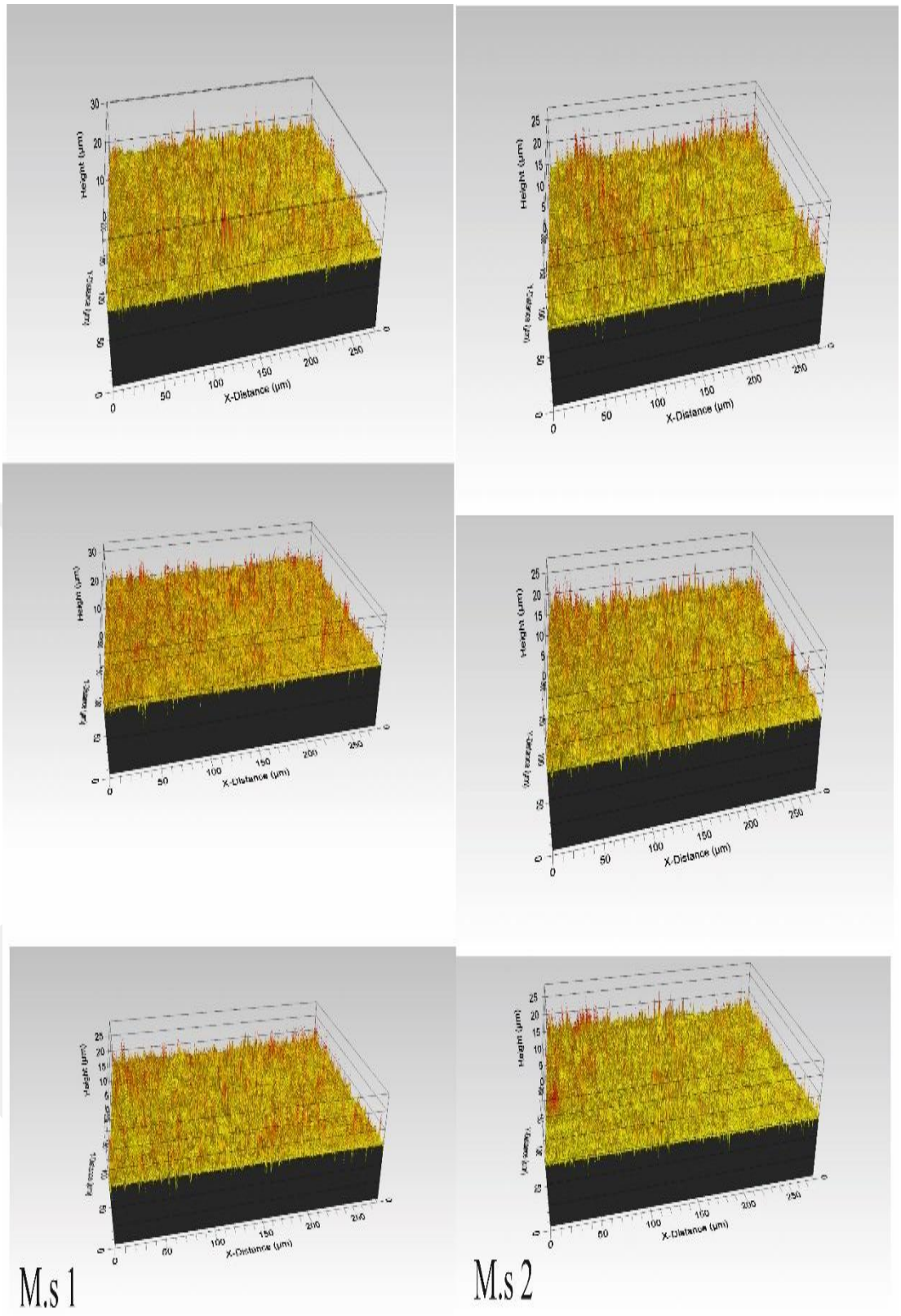

Figure 2. 27 Surface roughness analyzed image using AFM program for the firest and second machined surface

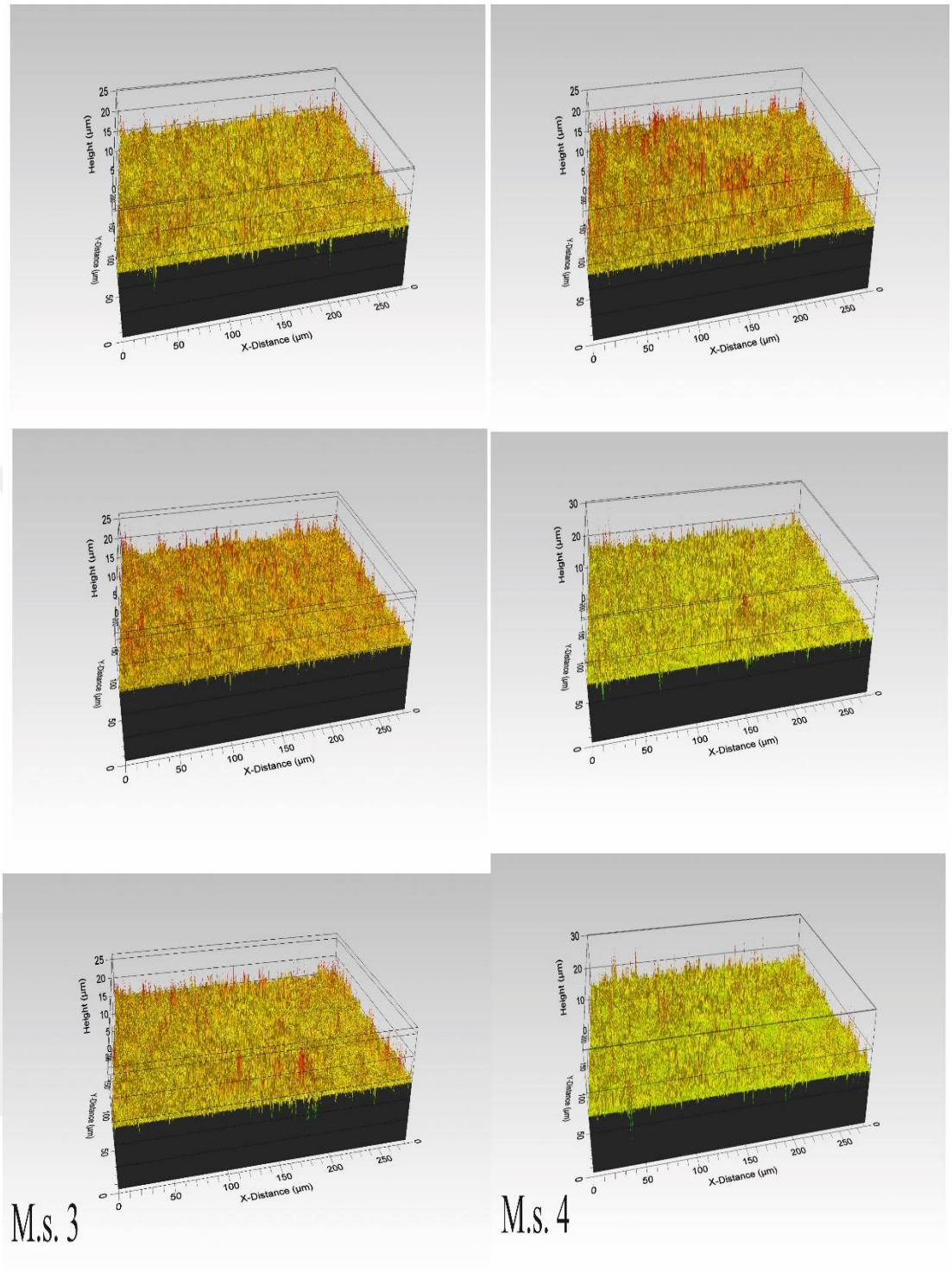

Figure 2. 28 Surface roughness analyzed image using AFM program for the third and forth machined surface

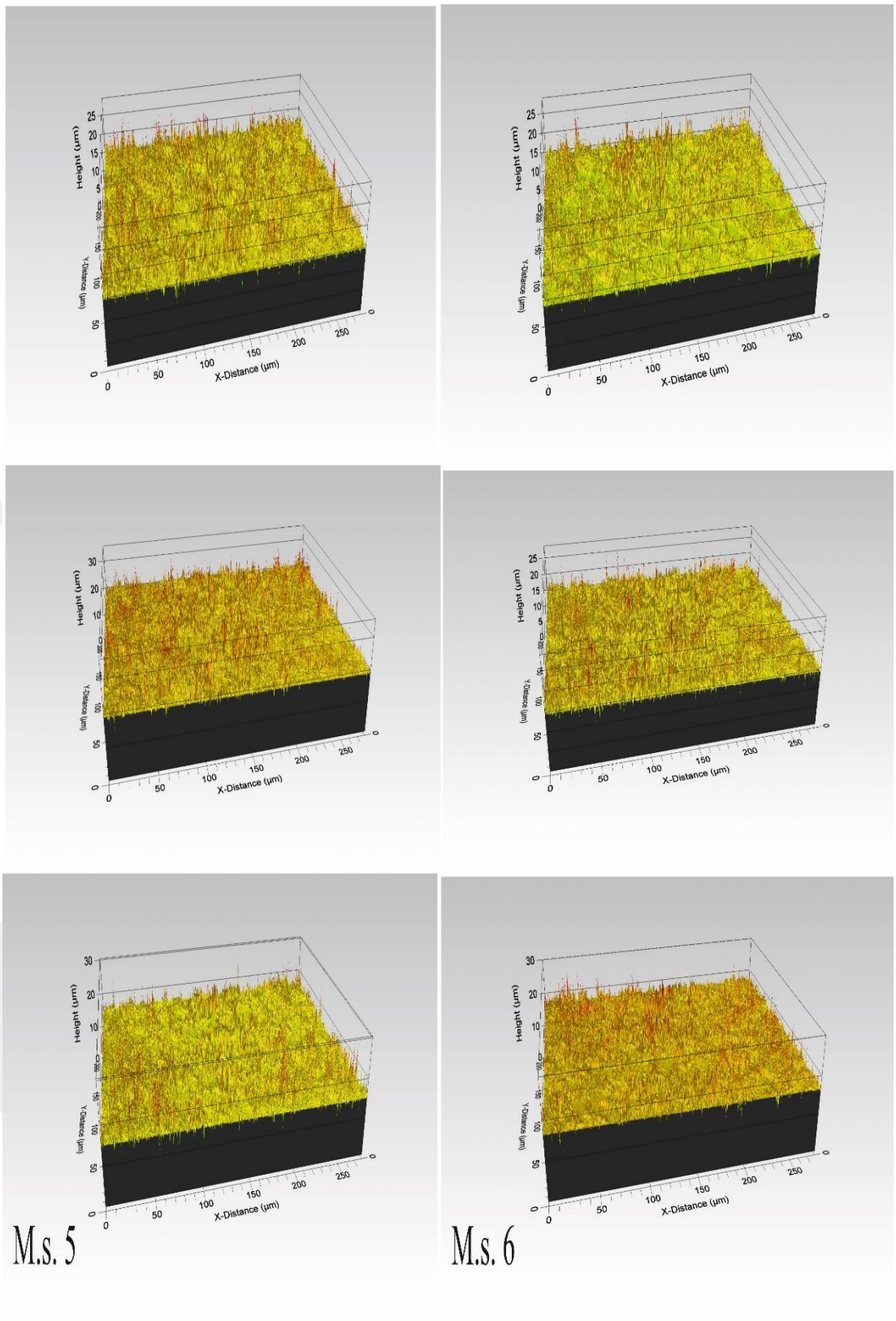

Figure 2. 29 Surface roughness analyzed image using AFM program for the fifth and sixth machined surface

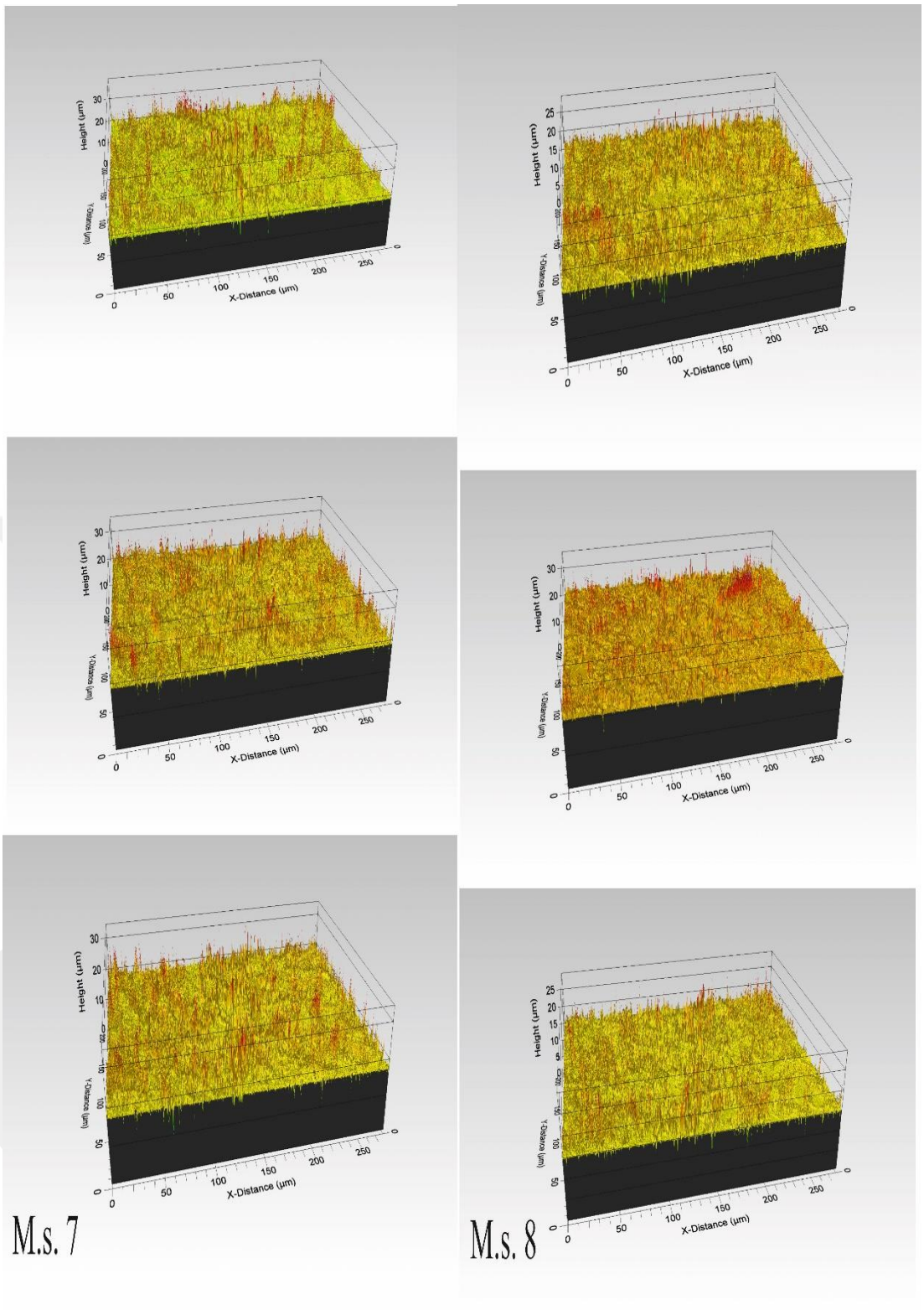

Figure 2. 30 Surface roughness analyzed image using AFM program for the seventh and eighth machined surface

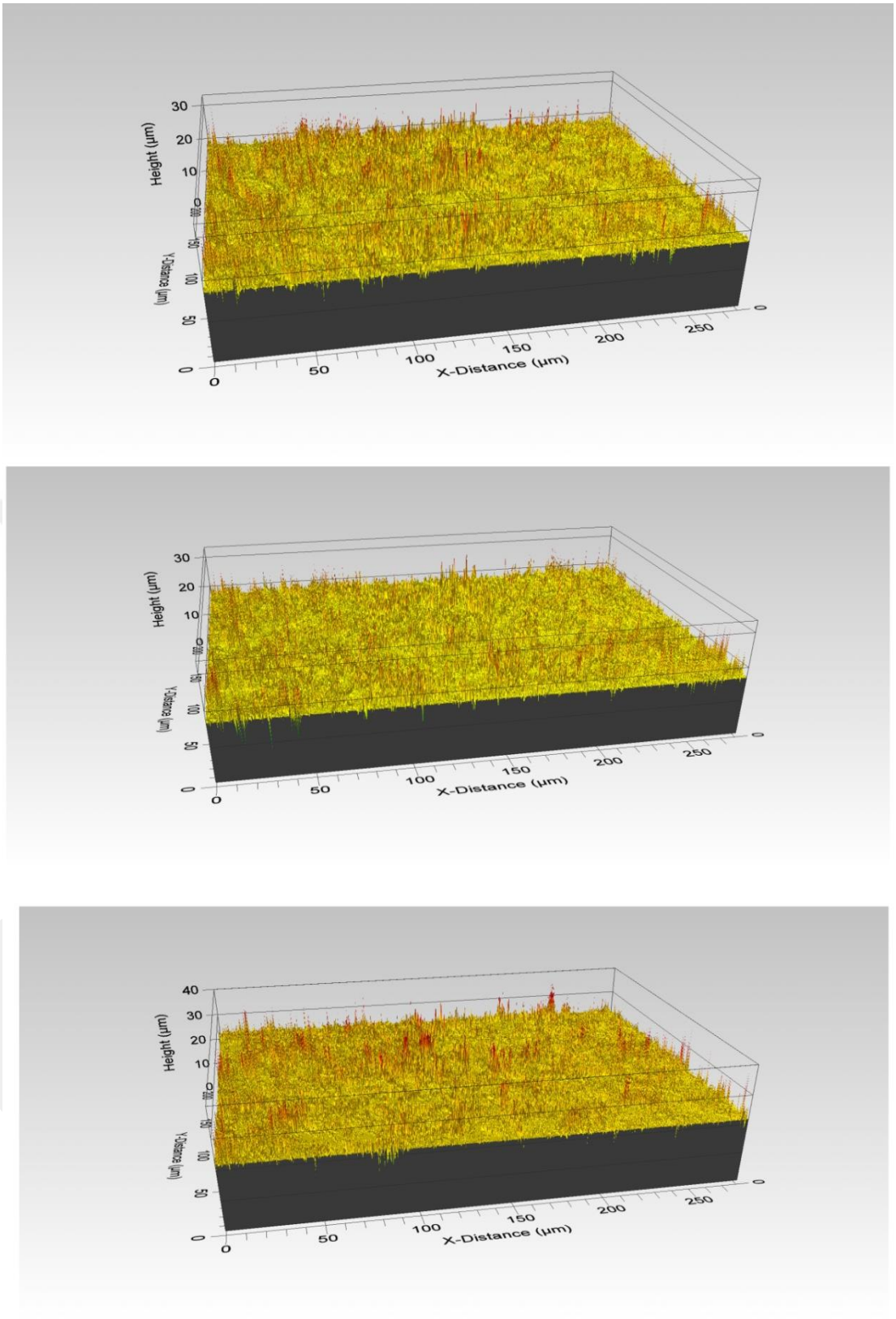

Figure 2. 31 Surface roughness analyzed image using AFM program for the ninth machined surface

2.3.6.3 Micro-hardness Measurement

Hardness is an important measurement for the study of the mechanical properties of recast layers having re-solidified on a machined surface. The hardness was found to be varying from the upper part of the machined surface inward deeply into the bulk material [41]. This change is due to the formation of new phases on the machined surface due to the interaction of some components such as titanium and nitrogen with oxygen and carbon and forming oxide and carbide components and re-solidifying on the surface. The area following the precipitated layer is a heat-affected zone, and as a result of the rapid cooling of the dielectric fluid, it becomes a mixed phase of martensite, austenite and the transformation phases. Due to the austenite phase in the heat-affected zone, the hardness of this area is higher than the bulk material.

Micro-Hardness tests on the Vickers scale were performed using a micro-hardness tester ZWICK.ROELL ZHvμ (Micro Manufacturing Laboratory, Bilkent University) equipped with a pyramidal diamond indenter 136° and a mass force of 1 kg within the test period of 10 seconds. Figure 2.32 shows the micro-hardness tester.

Figure 2. 32 Micro-hardness ZWICK.ROELL ZHv μ tester

The precision micro-hardness tester is calibrated using the value of the Brass Block Cage. The calibration result with a 1% error was considered in other tests, as shown in Figure 2.33, for accurate results.

Figure 2. 33 Micro-hardness ZWICK.ROELL ZHv μ calibration

The micro-hardness of the bulk material was 195 Vickers, which was ground, polished and etched, as illustrated in Section 2.3.3, was measured by taking an average of five readings that were to be compared with the micro-hardness of other machined surfaces later, as shown in Figure 2.34.

Figure 2. 34 Measuring of bulk material micro-hardness

Nitinol samples, before measuring the microhardness, were fixed onto an aluminum fixture into which nine holes were drilled using a milling machine. The samples were then placed in those holes and installed with a strong adhesive to prevent the samples from sliding under the indenter during the tests so as to avoid errors in the readings. The micro-hardness of the nine machined surfaces was measured in five readings each at different locations on each surface (see Figure 2.19).

CHAPTER 3

Design of The Experiments and Results Analyses

3.1 Design of the Experiment

In order to study the effect of the μ-WEDM cutting process parameters, twenty-seven experiments were performed to determine which parameters had a significant impact on surface integrity.

In this work, the Taguchi orthogonal array (L_{27}) was selected to design the experiments. Four adjustable parameters, namely peak current, pulse on time, pulse off time and servo voltage with three levels for each parameter (Table 2.1, Chapter 2), were selected and the remainder were fixed (Table 2.2, Chapter 2). A set of pilot experiments were performed to determine the range values of the parameter levels to avoid short-circuits, which inevitably leads to cutting of the wire between the cutting wire and the workpiece during the erosion process.

Table 3.1 illustrates that the design of the DOE includes of the input parameter levels and their distribution method according to the Taguchi orthogonal array (L_{27}) and the measured output responses of the machined surface of the Nitinol sample as, explained in Chapter 2.

Based on the orthogonal Taguchi array L_{27}, a surface response methodology (Eq. 3.1) [42] was applied to analyze measured data with a 95% confidence level using the Minitab software. Optimization analysis of the levels of the cutting parameters was also performed to achieve the best result for the output responses.

3.2 Response Surface Methodology

The Surface Response Methodology is a mixture of mathematical techniques and statistical methods designed to analyze absolved data for independent variables that affect dependent responses [43].

Table 3 1 Design of the experiments with Taguchi orthogonal array (L27)

Exp. No.	Input parameters levels				Measured output responses				
	On μs	Off μs	Ip A	Sv V	Kerf mm	MRR mm^3/min	WLT μm	Sa μm	Mh Vicker
1	3.5	5	0.6	80	0.24327	0.27144	3.7336	0.3326	430
2	3.5	5	0.6	80	0.24275	0.27086	4.283	0.3433	418
3	3.5	5	0.6	80	0.24103	0.26894	4.325	0.3177	306
4	3.5	10	6	130	0.23939	0.27923	4.3115	0.3269	495
5	3.5	10	6	130	0.23978	0.27968	3.75275	0.3019	411
6	3.5	10	6	130	0.23811	0.27774	4.0172	0.3062	419
7	3.5	16	11	180	0.24412	0.06612	3.7286	0.295	403
8	3.5	16	11	180	0.2444	0.0662	3.67975	0.2798	333
9	3.5	16	11	180	0.24235	0.06564	4.07767	0.2729	312
10	5	5	6	180	0.24367	0.17983	4.95783	0.304	535
11	5	5	6	180	0.24388	0.17999	4.6734	0.3115	469
12	5	5	6	180	0.24217	0.17872	4.333	0.3202	482
13	5	10	11	80	0.23634	0.35418	4.8024	0.2982	587
14	5	10	11	80	0.23628	0.35408	4.8118	0.3042	691
15	5	10	11	80	0.23461	0.35158	4.585	0.2835	643
16	5	16	0.6	130	0.23978	0.20278	3.76783	0.2591	472
17	5	16	0.6	130	0.23925	0.20233	4.043	0.2373	470
18	5	16	0.6	130	0.2376	0.20094	4.17667	0.2656	495
19	7.5	5	11	130	0.24057	0.55272	3.2471	0.3487	611
20	7.5	5	11	130	0.23922	0.54961	2.6515	0.375	571
21	7.5	5	11	130	0.24052	0.55261	3.1546	0.3767	615
22	7.5	10	0.6	180	0.24732	0.11845	7.1066	0.2835	484
23	7.5	10	0.6	180	0.24793	0.11874	7.104	0.3045	497
24	7.5	10	0.6	180	0.24608	0.11785	6.6598	0.2864	515
25	7.5	16	6	80	0.23617	0.24265	5.0668	0.328	551
26	7.5	16	6	80	0.23641	0.2429	4.6055	0.3196	443
27	7.5	16	6	80	0.23503	0.24149	4.84	0.3216	460

According to the central composite design (CCD) of the response surface methodology, it is possible to generate an approximated model based on either the measured data or the observed data. This model is an empirical model after applying the multiple regression analysis, which is a statistical technique dedicated to obtain these types of experimental models.

$$Y = a_0 + \sum_{j=1}^{k} a_j x_j + \sum_{j=1}^{k} a_{jj} x_j^2 + \sum_{i<j} \sum_{j=2}^{k} a_{ij} x_i x_j \quad (3.1)$$

where the factors a_0, a_j, a_{jj}, a_{ij} = 0, 1, …, k are named the regression coefficients. Second-order experimental models were generated for every response studied based on the observed data.

3.3 Optimization Analyses Approaches

In this study, two algorithms were used in the optimization analysis to compare and validate the results, namely the gradient algorithm and particle swarm optimization algorithm

3.3.1 Gradient Algorithm

he optimization analysis was performed using a gradient algorithm (Eqs. 3.2-3.4) [42].

The gradient algorithm was used to convert individual or combined responses into desirability indices. The transformation is achieved by performing the following steps, as shown in Equations 3.2-3.4.

Step 1: The Individual Desirability Index (y_i) for each response is calculated according to the required state of the response, either to increase or decrease the response or to achieve a specific target.

If the response is required to achieve the maximum, in this case, Equation 3.2 is used.

$$\left.\begin{array}{ll} y_i = 0 & i < S_i \\ y_i = [(i - S_i)/(H_i - S_i)]^{ri} & S_i \leq i \leq H_i \\ y_i = 1 & i > H_i \end{array}\right\} \quad (3.2)$$

If the response is required to achieve the minimum, in this case Equation 3.3 is used.

$$\left.\begin{array}{ll} y_i = 0 & i > H_i \\ y_i = [(H_i - i)/(H_i - S_i)]^{ri} & S_i \leq i \leq L_i \\ y_i = 1 & i < S_i \end{array}\right\} \quad (3.3)$$

If the response is required to achieve a specified target, in this case, Equation 3.4 is used.

$$\left.\begin{array}{ll} y_i = 0 & i < S_i \\ y_i = [(i - S_i)/(T_i - S_i)]^{ri} & S_i \leq i \leq L_i \\ y_i = [(i - H_i)/(T_i - H_i)]^{ri} & S_i \leq i \leq H_i \\ y_i = 0 & i > H_i \end{array}\right\} \quad (3.4)$$

where y_i = the individual desirability for the i^{th} response, i = the predicted value of the i^{th} response, S_i = the smallest acceptable value for the i^{th} response, H_i = the highest acceptable value for the i^{th} response and r^i = the weight exponent.

Step 2: In case we have many individual responses and are required to have a combined desirability index for all of them, then Equation 3.5 will be applied after acquiring each individual desirability index for each output response separately.

$$D = \left(y_1^{w_1} * y_2^{w_1} * \dots\dots\dots\dots * y_n^{w_n}\right)^{1/\sum_{j=1}^{n} w_j} \quad (3.5)$$

$$Y = \frac{1}{1+D} \quad (3.6)$$

where D = the global desirability index, n = the total number of response parameters, w_i = the individual weight of the j^{th} response and Y = the fitness function (Eq. 3.6).

3.3.2 Particle Swarm Optimization (PSO)

PSO is a random arithmetic search and modulation method that relies on the movement and intelligence of swarms to find items while searching for specific targets such as food within a specific search space [44].

The idea of the algorithm is based on the solutions provided by each of the swarm particles based on the local experience gained and global experience with the neighbors' particles within the swarm and provides the best solution over time to achieve the desired goal or the best result within the research space. This algorithm relies on the experience gained, memory and time during the search process in a given space [42].

The three methods in the Particular Swarm Optimization category, namely Particle Swarm Optimization-Original (PSO-O) [45, 46], Particle Swarm Optimization-Inertia Weight (PSO-IW) [47] and Particle Swarm Optimization-Constriction Factor (PSO-CF) [47], were used in this study based on the empirical model generated by the surface response methodology. The results were identical, except for the difference in the number of iterations to reach the desired goal. The steps used in the algorithm are shown in Figure 3.1.

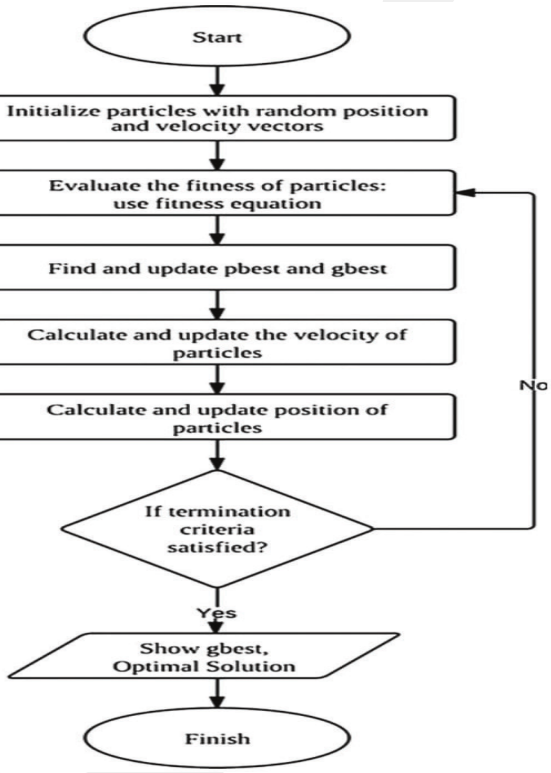

Figure 3. 1 Flow Chart of PSO[48]

Assuming that a swarm has a certain space and that they want to conduct a search on a certain goal in that space, which has d dimensions and they have the i^{th} particle of a swarm represented by a d-dimensional position $x_i = (x_{i1}, x_{i2}, \ldots..., x_{id})$, the velocity of the particle can be defined by $vi = (v_{i1}, v_{i2}, \ldots., v_{id})$. Moreover, the best visited position for the i^{th} particle would be p_{id} and the best position visited by one of the other particles would be g_{id}. The updated positions will be based on one of the following methods explained below.

3.3.2.1 Particle Swarm Optimization-Original (PSO-O)

The new position and velocity of each particle will be determined according to the following equations:

$$v_{id}^{j+1} = v_{id}^{j} + c_1 \, x \, r_1 \, x \, \left(p_{id} - x_{id}^{j}\right) + \, c_2 \, x \, r_2 \, x\left(g_{id} - x_{id}^{j}\right) \tag{3.7}$$

$$x_{id}^{j+1} = x_{id}^{j} + v_{id}^{j+1} \tag{3.8}$$

where the Cognitive parameter C1 = 2 [50, 51], the social parameter C2 = 2 [50, 51], r_1 and r_2 are random numbers uniformly distributed in the range [0-1], and j = 1, 2… is the current iteration.

3.3.2.2 Particle Swarm Optimization- Inertia Weight (PSO-IW)

The new position and velocity of each particle are determined according to the following equations:

$$v_{id}^{j+1} = w \, x \, v_{id}^{j} + c_1 \, x \, r_1 \, x \, \left(p_{id} - x_{id}^{j}\right) + \, c_2 \, x \, r_2 \, x\left(g_{id} - x_{id}^{j}\right) \tag{3.9}$$

$$x_{id}^{j+1} = x_{id}^{j} + v_{id}^{j+1} \tag{3.10}$$

$$w = \, w_{max} - \frac{w_{max} - w_{min}}{N_{max}} \, x \, iter \tag{3.11}$$

where w (inertia weight) is calculated using Equation 3.11. As the proportional agent, w is related to the previous velocity. The cognitive parameter is C1 = 2 [49, 50], the social parameter is C2 = 2 [49, 50] and r1 and r2 are random numbers uniformly distributed in the range [0-1]; j = 1, 2,… is the current iteration. The initial weight w_{max} = 0.9 [51], the final weight w_{min} = 0.4 and N_{max} = the maximum number of iterations.

3.3.2.3 Particle Swarm Optimization- Constriction Factor (PSO-CF)

This method with constriction agents was first introduced by Clerc, M. et al. in their research paper [52]. The new position and velocity of each particle is determined according to the following equations:

$$v_{id}^{j+1} = k\{v_{id}^{j} + c_1 \, x \, r_1 \, x \, \left(p_{id} - x_{id}^{j}\right) + \, c_2 \, x \, r_2 \, x\left(g_{id} - x_{id}^{j}\right)\} \tag{3.12}$$

$$x_{id}^{j+1} = x_{id}^{j} + v_{id}^{j+1} \tag{3.13}$$

$$k = \frac{2}{|2 - c - \sqrt{c^2 - 4c}|} \tag{3.14}$$

where k is the constriction factor (Eq. 3.14), $C = C_1 + C_2$, the cognitive parameter $C_1 = 2$ [49, 50], and the social parameter $C_2 = 2$ [49, 50]; r_1 and r_2 are random numbers uniformly distributed in the range [0-1] and $j = 1, 2,\ldots$ is the current iteration. Appendix A shows the MATLAB code which was designed to calculate the particle swarm algorithm.

3.4 Analysis of Variance (ANOVA) and Optimizations

Multiple regression analysis was carried out to determine the relationship between the μ-WEDM cutting parameters and the studied responses, which included surface integrity responses, metal removal rate "MRR", and Kerfs variation.

In this study, all analyses of variance were performed according to a 95% confidence level ($\alpha = 0.05$). R^2 was calculated to determine the fit in the regression model [53, 54]. R^2 demonstrates how well an accurate expected result can be achieved using all the input parameters in the model, while an adjusted R^2 shows how an accurate result can be achieved using only the significant input parameters in the model. If the difference between $R^2$and an adjusted adj-R^2 is more than 0.2, this causes the model to be insignificant or the data entered wrongly interpreted in the program [55].

The sequential sums of squares (Seq SS) measure the reduction in the residual sums of squares provided by each term in the model. The adjusted sums of squares (Adj SS) measures the reduction in the residual sums of squares provided by each term relative to a model containing all the other terms. The adjusted mean square (Adj MS) values are adjusted sums of squares (Adj SS) divided by the corresponding DF. The F ratio or F-test is the statistical test used to decide whether the model altogether has a statistically significant predictive capability. F is the ratio of the model mean square to the error mean square. The p values tell whether a term has statistically significant predictive capability in the presence of the other variables. The values of F, p, and R^2can be used to study the regression model as a whole in addition to the most significant coefficients [53].

3.4.1 Kerf Variation

The analysis of Variance (ANOVA) of the Kerf variation was performed using the surface response methodology on the Minitab 16.2.4 software with a 95% confidence level, as shown in Table 3.2

The regression model of the Kerf variation was constructed with 8 DF using the response surfaces methodology "desirability function approach," as shown in Equation 3.15 after regression analysis was performed, as shown in Table 3.2.

The correlation coefficients for this model are R^2 and adj-R^2 valued at 0.9522 and 0.9310, respectively. The difference between R^2 and adj-R^2 is less than 0.2, so the predictive capability of the regression model is significant. Moreover, there is reasonable agreement between the adjusted R^2 value of 0.9310 and the predictive R^2 value of 0.8925, which shows that the experimental and predicted data for the regression model are consistent.

$$\begin{aligned}\text{Kerf variation} = {} & 0.271249 - 0.00648521 * \text{On} - 3.19560\text{E} - 04 * \text{Off} - 0.00232323 \\ & * \text{Ip} - 1.37654\text{E} - 04 * \text{Sv} + 0.000574513 * \text{On}^2 + 4.64791\text{E} - 06 \\ & * \text{Off}^2 + 0.000132975 * \text{Ip}^2 + 7.86001\text{E} - 07 * \text{Sv}^2\end{aligned} \tag{3.15}$$

Table 3.2 shows the ANOVA of the kerf variation, which was performed at a 95% confidence level. From these results, it can be observed that the F-test value is 45 and the p-value (alpha) is < 0.05 for the kerf variation regression model. Thus, the F and p-values indicate that the regression model has statistical significance and a large predictive capability.

The ANOVA analysis of the Kerf variation in Table 3.2 shows that the most effective μ-WEDM cutting parameters influencing the Kerfs are servo voltage and peak current, respectively, in which their p-values are < 0.05 and F-test values are 212 and 42, respectively. Moreover, it was found that the pulse off time was the third significant parameter affected by Kerf variation with a p-value of 0, while the pulse on time was insignificant with a p-value of > 0.05.

Table 3 2 ANOVA of Kerf Variation

Source	DF	Seq SS	Adj SS	Adj MS	F	P
Regression	8	0.000339	0.000339	0.000042	44.85	0.000
Linear	4	0.000255	0.000268	0.000067	71.03	0.000
ON	1	0.000002	0.000002	0.000002	2.09	0.166
OFF	1	0.000027	0.000000	0.000000	28.39	0.000
IP	1	0.000028	0.000039	0.000039	41.66	0.000
Sv	1	0.000200	0.000200	0.000200	211.96	0.000
Square	4	0.000084	0.000084	0.000021	22.15	0.000
ON*ON	1	0.000027	0.000027	0.000027	28.88	0.000
OFF*OFF	1	0.000000	0.000000	0.000000	0.12	0.730
IP*IP	1	0.000033	0.000033	0.000033	35.09	0.000
Sv*Sv	1	0.000023	0.000023	0.000023	24.52	0.000
Residual Error	18	0.000017	0.000017	0.000001		
Pure Error	18	0.000017	0.000017	0.000001		
Total	26	0.000356				

A single response optimization was performed to determine the best μ-WEDM cutting parameters that lead to reducing of the Kerf variation on the machined surface of the workpiece by using the gradient algorithm (individual desirability), as explained in Equations 3.2 to 3.6, which are provided by the surface response methodology in the Minitab software.

Figure 3.2 shows the optimum μ-WEDM cutting parameters for the minimum kerf width, followed by the extracted result being compared with the Particle Swarm Optimization algorithm (PSO) results for the same kerf variation regression model in order to obtain an accurate result. The PSO is explained with Equations 3.7 to 3.14. Table 3.3 shows the comparative results of optimum μ-WEDM cutting parameters for the minimum Kerf width. However, the difference in the minimum kerf widths, and the optimum cutting parameters values is almost negligible between the two algorithms.

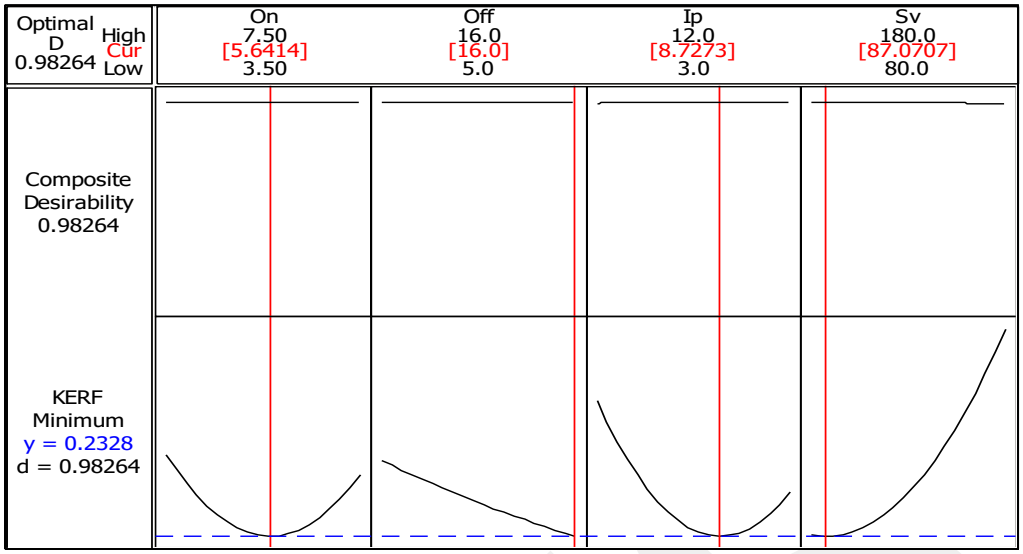

Figure 3. 2 Optimum µ-WEDM cutting parameters for minimum kerf width

Table 3 3 Optimum Cutting Parameters for Minimum Kerf Width

parameters	d. index = 0.982643	PSO
Pulse on time (Ton) µs	5.64141	5.62081
Pulse off time(Toff) µs	16	16
Peak current (Ip) A	8.72727	8.73002
Servo voltage (Sv) V	87.0707	80
Kerf Width (mm)	0.232850	0.23290

3.4.2 Metal Removed Rate (MRR)

A variance analysis (ANOVA) of the metal removal rate (MRR) was performed using the surface response methodology on the Minitab 16.2.4 software with a 95% confidence level, as shown in Table 3.4.

The regression model of the MRR was constructed with 8 DF using the response surfaces methodology (desirability function approach), as shown in Equation 3.16 after the regression analysis was performed, as shown in Table 3.4.

The correlation coefficients in this model for R^2 and adj-R^2 are 1 and 0.9999, respectively. The difference between R^2 and adj-R^2 is proximity zero, so the predictive capability of the regression model is significant. Moreover, there is high agreement between the adjusted R^2 value of 0.9999 and the predictive R^2 value of 0.9999, which shows that the experimental and predicted data for the regression model are identical.

$$\text{MRR} = (-0.435038) + 0.0327070 * \text{On} - 0.0213667 * \text{Off} + 0.00942807 * \text{Ip} + 0.0128029 * \text{Sv} - 7.22974\text{E} - 04 * \text{On}^2 + 0.000308625 * \text{Off}^2 + 0.000310072 * \text{Ip}^2 - 5.56803\text{E} - 05 * \text{Sv}^2 \quad (3.16)$$

Table 3.4 shows the ANOVA of the MRR, which was performed at a 95% confidence level. From the results, it can be observed that the F-test value is very high and the p-value (alpha) is zero for the MRR regression model. Thus, the F and p-values indicate that the regression model has statistical significance and large predictive capability.

ANOVA analysis of the MRR in Table 3.4 shows that the most effective μ-WEDM cutting parameters influencing the MRR are servo voltage, pulse off time, pulse on time and peak current, respectively, where their p-values are zero, and F-test values are very, high as shown in Table 3.4.

Table 3 4 ANOVA of Metal Removed Rate (MRR)

Source	DF	Seq SS	Adj SS	Adj MS	F	P
Regression	8	0.484242	0.484242	0.060530	52974.89	0.000
Linear	4	0.367245	0.363123	0.090781	79449.6	0.000
ON	1	0.044637	0.044120	0.044120	38612.89	0.000
OFF	1	0.120158	0.120651	0.120651	105591.3	0.000
IP	1	0.076349	0.072252	0.072252	63233.6	0.000
Sv	1	0.126100	0.126100	0.126100	110360.6	0.000
Square	4	0.116997	0.116997	0.029249	25598.45	0.000
ON*ON	1	0.000043	0.000043	0.000043	37.81	0.000
OFF*OFF	1	0.000513	0.000513	0.000513	448.91	0.000
IP*IP	1	0.000180	0.000180	0.000180	157.73	0.000
Sv*Sv	1	0.116261	0.116261	0.116261	101749.3	0.000
Residual Error	18	0.000021	0.000021	0.000001		
Pure Error	18	0.000021	0.000021	0.000001		
Total	26	0.484263				

A single response optimization was performed to determine the best μ-WEDM cutting parameters that lead to increasing the MRR by using the gradient algorithm (individual

desirability), as explained in Equations 3.2 to 3.6, which are provided by the surface response methodology in the Minitab software.

Figure 3.5 shows the optimum µ-WEDM cutting parameters for maximum MRR, followed by the extracted result being compared with the PSO results for the same MRR regression model to obtain an accurate result. The PSO is explained by Equations 3.7 to 3.14. Table 3.5 shows the comparative results of the optimum µ-WEDM cutting parameters for maximum MRR. However, the difference between the maximum MRR and the optimum cutting parameters values are almost negligible between the two algorithms.

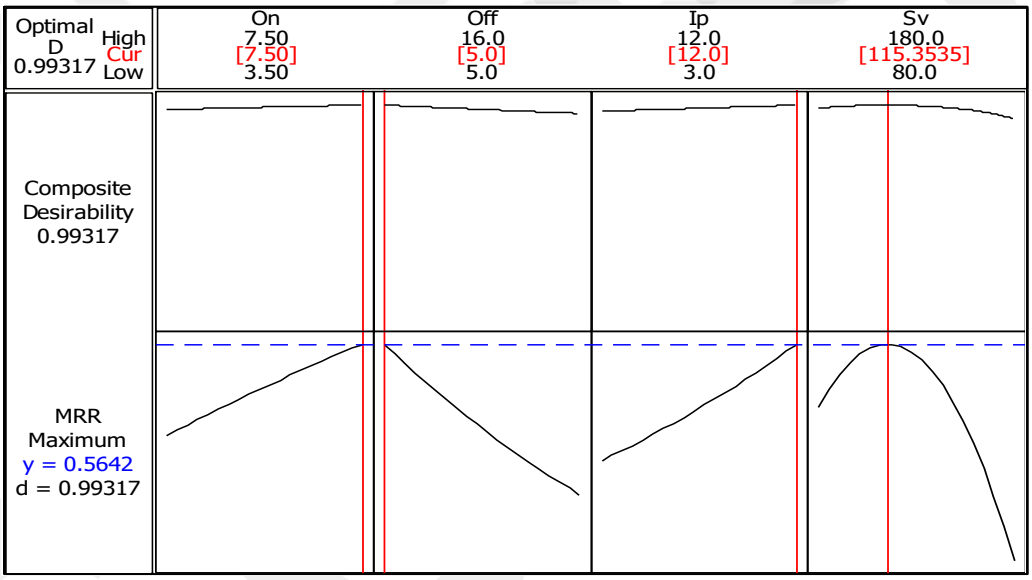

Figure 3. 3 Optimum µ-WEDM Cutting Parameters for Maximum MRR.

Table 3 5 Optimum µ-WEDM Cutting Parameters for Maximum MRR

parameters	d. index = 0.993168	PSO
Pulse on time (Ton) µs	7.5	7.5
Pulse off time(Toff) µs	5	5
Peak current (Ip) A	12	12
Servo voltage (Sv) V	115.354	114. 96554
MRR (mm/min)	0.564219	0.56423

3.4.3 White Layer Thickness (W.L.T)

The variance analysis (ANOVA) of the White Layer Thickness (W.L.T.) was carried out using the surface response methodology on the Minitab 16.2.4 software with a 95% confidence level, as shown in Table 3.6.

The regression model of the W.L.T was built with 8 DF using the response surfaces methodology "desirability function approach," as shown in Equation 3.17 after regression analysis was performed, as shown in Table 3.6.

The correlation coefficients for R^2 and adj-R^2 are 0.9587 and 0.9403, respectively. The difference between R^2 and adj-R^2 is 0.02, so the predictive capability of the regression model is significant. Additionally, there is high agreement between the adjusted R^2 value of 0.9403 and the predictive R^2 value of 0.9070, which shows that the experimental and predicted data for the regression model are consistent.

$$\boldsymbol{W.L.T} = 6.13701 + 0.577222 * \mathrm{On} + 0.850824 * \mathrm{Off} - 0.236046 * \mathrm{Ip} - 0.116228 * \mathrm{Sv} - 0.0309423 * \mathrm{On}^2 - 0.0392519 * \mathrm{Off}^2 + 0.00712647 * \mathrm{Ip}^2 + 0.000469543 * \mathrm{Sv}^2 \quad (3.17)$$

Table 3.6 shows the ANOVA of the W.L.T. which was performed at a 95% confidence level. From these results, it can be observed that the F-test value is 52 and the p-value (alpha) is zero for the W.L.T. regression model. Thus, the F and p-values indicate that the regression model has statistical significance and a large predictive capability.

The ANOVA analysis of the W.L.T. in Table 3.6 shows that the most effective μ-WEDM cutting parameters influencing the W.L.T. are peak current and servo voltage, respectively. where their p-values are ~ 0 and F-test values are 89 and 22. It was found that the pulse on time was the third significant parameter affecting on W.L.T. with a p-value of zero, which is < 0.05, while the pulse off time was a little below 0.05. Its significance comes in last place with a p-value of > 0.029.

Table 3 6 ANOVA of White Layer Thickness (W.L.T)

Source	DF	Seq SS	Adj SS	Adj MS	F	P
Regression	8	28.470600	28.470600	3.558830	52.17	0.000
Linear	4	11.731600	12.043800	3.010950	44.13	0.000
ON	1	4.039300	0.304500	0.304460	4.46	0.000
OFF	1	0.219800	0.383300	0.383330	5.62	0.029
IP	1	6.010200	6.079700	6.079680	89.12	0.000
Sv	1	1.541500	1.541500	1.541500	22.6	0.000
Square	4	16.739000	16.739000	4.184750	61.34	0.000
ON*ON	1	0.079100	0.079100	0.079130	1.16	0.296
OFF*OFF	1	28.470600	28.470600	3.558830	52.17	0.000
IP*IP	1	0.095200	0.095200	0.095200	1.4	0.253
Sv*Sv	1	8.267700	8.267700	8.267700	121.19	0.000
Residual Error	18	1.228000	1.228000	0.068220		
Pure Error	18	1.228000	1.228000	0.068220		
Total	26	29.6986				

A single response optimization was performed to determine the best μ-WEDM cutting parameters that lead to a reduction in the W.L.T using the gradient algorithm "individual desirability," as explained in Equations 3.2 to 3.6, which are provided by the surface response methodology in the Minitab software.

Figure 3.4 shows the optimum μ-WEDM cutting parameters for minimum W.L.T., followed by the extracted result being compared with the PSO results for the same W.L.T. regression model to obtain an accurate result. The PSO is explained using Equations 3.7 to 3.14.

Table 3.7 shows comparative results of optimum μ-WEDM cutting parameters for minimum W.L.T. However, the difference in the minimum W.L.T. and the optimum cutting parameter values are almost negligible between both algorithms.

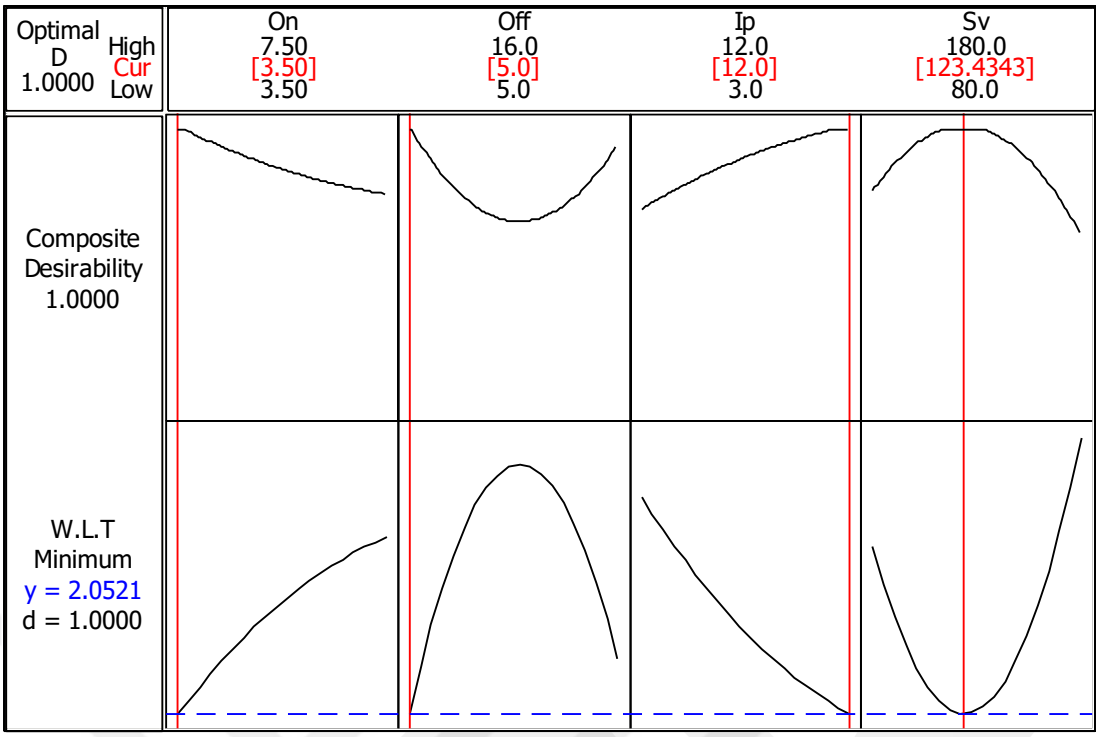

Figure 3. 4 Optimum µ-WEDM cutting parameters for minimum W.L.T.

Table 3 7 Optimum µ-WEDM cutting parameters for minimum W.L.T

parameters	d. index =1.0	PSO
Pulse on time (Ton) µs	3.5	3.5
Pulse off time(Toff) µs	5	5
Peak current (Ip) A	12	12
Servo voltage (Sv) V	123.434	123. 76952
W.L.T (µm)	2.05212	2.05212

3.4.4 Surface Roughness (Sa)

A variance analysis (ANOVA) of the Surface Roughness (Sa) was performed using the surface response methodology on the Minitab 16.2.4 software with a 95% confidence level, as shown in Table 3.8. Average arithmetic height (Ra) is the most common term used to describe surface roughness in the industrial fields. Therefore, it is relied upon here to describe the degree of surface roughness according to ISO 251778.

The regression model of the Sa was built with 6 DF using the response surfaces methodology (desirability function approach), as shown in Equation 3.18, after regression analysis was performed (see Table 3.8).

For this model, the correlation coefficients R^2 and adj-R^2 are 0. 9019 and 0.8657, respectively. The difference between R^2 and adj-R^2 is < 0.04, so the predictive capability of the regression model is significant. Moreover, there is reasonable agreement between the adjusted R^2 value of 0.8657 and the predictive R^2 value of 0.8066, which shows that the experimental and predicted data for the regression model are consistent.

$$\begin{aligned} \mathrm{Sa} = {} & 0.554337 - 0.0786443 * \mathrm{On} - 0.0146251 * \mathrm{Off} + 0.0156574 * \mathrm{Ip} \\ & - 2.12111\mathrm{E} - 04 * \mathrm{Sv} + 0.00757296 * \mathrm{On}^2 + 0.000479596 * \mathrm{Off}^2 \\ & - 8.75926\mathrm{E} - 04 * \mathrm{Ip}^2 \end{aligned} \tag{3.18}$$

Table 3.8 shows the ANOVA of the Sa, which was performed at a 95% confidence level. From these results, it can be observed that the F-test value is 25 and the p-value (alpha) is zero for the Sa regression model. Thus, the F and p-values indicate that the regression model has statistical significance and large predictive capability.

The ANOVA analysis of the Sa in Table 3.8 shows that the most effective µ-WEDM cutting parameters influencing the Sa are pulse off time and peak current, where, their p-values ~ 0 and F-test values are 80, and 16 respectively. It was also found that the servo voltage and pulse on time were the third and forth significant parameters affecting the Sa with a p-value of 0.001 and 0.004, respectively. Since the values of the F-test are somewhat close, the lack of fit is not significant in the regression model when its p-value is greater than 0.05. Here the p-value for lack of fit was 0.324 and the F-test value is very low, approximately 1 at most.

A single response optimization was performed to determine the best µ-WEDM cutting parameters that lead to reducing the Sa by using the gradient algorithm (individual desirability), as explained in Equation 3.2 to 3.6, which are provided by the surface response methodology in the Minitab software.

Table 3 8 ANOVA of Surface Roughness (Sa)

Source	DF	Seq SS	Adj SS	Adj MS	F	P
Regression	7	0.024597	0.024597	0.003514	24.95	0.000
Linear	4	0.017180	0.017189	0.004297	30.51	0.000
ON	1	0.002487	0.001562	0.001562	11.09	0.004
OFF	1	0.010931	0.011290	0.011290	80.16	0.000
IP	1	0.001736	0.002312	0.002312	16.41	0.001
Sv	1	0.002025	0.002025	0.002025	14.37	0.001
Square	3	0.007417	0.007417	0.002472	17.55	0.000
ON*ON	1	0.004740	0.004740	0.004740	33.65	0.000
Off*Off	1	0.001239	0.001239	0.001239	8.79	0.008
IP*IP	1	0.001438	0.001438	0.001438	10.21	0.005
Residual Error	19	0.002676	0.002676	0.000141		
Lack-of-Fit	1	0.000144	0.000144	0.000144	1.03	0.324
Pure Error	18	0.002532	0.002532	0.000141		
Total	26	0.027273				

Figure 3.5 shows the optimum μ-WEDM cutting parameters for the minimum Sa, followed by the extracted result being compared with the PSO results for the same Sa regression model to obtain an accurate result. The PSO algorithm is explained using Equations 3.7 to 3.14.

Table 3.9 shows comparative results of the optimum μ-WEDM cutting parameters for the minimum Sa. However, the difference between the minimum Sa and the optimum cutting parameter values are almost negligible between the two algorithms.

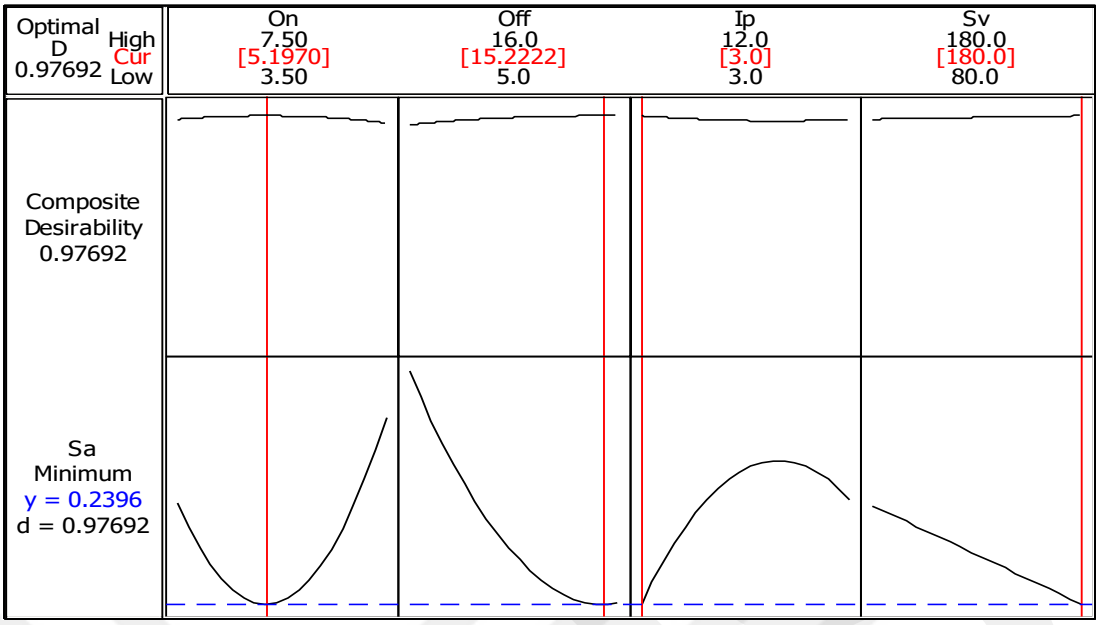

Figure 3. 5 Optimum µ-WEDM cutting parameters for minimum Sa

Table 3 9 Optimum µ-WEDM cutting parameters for minimum Sa

parameters	d. index =0.976916	PSO
Pulse on time (Ton) µs	5.19697	5.13421
Pulse off time(Toff) µs	15.2222	15.15309
Peak current (Ip) A	3	3
Servo voltage (Sv) V	180	180
Sa (µm)	0.23957	0.23960

3.4.5 Micro-hardness (Mh)

The variance analysis (ANOVA) of Micro-hardness (Mh) was performed using the surface response methodology on the Minitab 16.2.4 software with a 95% confidence level, as shown in Table 3.8.

The regression model of the Mh was built with 6 DF using the response surfaces methodology (desirability function approach), as shown in Equation 3.19 after the regression analysis was performed, as shown in Table 3.10.

The correlation coefficients for R^2 and adj-R^2 are 0.8287 and 0.7773, respectively. The difference between R^2, and adj-R^2 is 0.05, so the predictive capability of the regression model is significant. In addition, there is a reasonable agreement between the adjusted R^2 value of 0.7773 and the predictive R^2 value of 0.6828, which shows that the experimental and predicted data for the regression model are consistent.

$$Mh = (-507.860) + 314.022 * \text{On} + 36.2980 * \text{Off} + 8.51058 * \text{Ip} - 0.554444 * \text{Sv} - 25.4667 * \text{On}^2 - 1.96801 * \text{Off}^2 \quad (3.19)$$

Table 3.10 shows the ANOVA of the Mh, which was performed at a 95% confidence level. From the results, it can be observed that the F-test value is 16; the p-value (alpha) is zero for the Mh regression model. Thus, the F and p-values indicate that the regression model has a statistically significant predictive capability.

In the ANOVA analysis of the Mh, Table 3.10 shows that the most effective μ-WEDM cutting parameters influencing the Mh are pulse on time and peak current in which their p-values and F-test values are 41 and 13, respectively. It was found that servo voltage was the third significant parameter affecting the Mh with p-value 0.000, which is < 0.05 and F-test was 6.78. The pulse off time p-value was 0.017. Its significance comes in last place with the lowest F-test value of 6.75. The lack of fit is not significant on the regression model when its p-value is greater than 0.05. Here the p-value for the lack of fit was 0.242 and the F-test value is very low, at approximately 1.5 at most.

Table 3 10 ANOVA of micro-hardness (Mh)

Source	DF	Seq SS	Adj SS	Adj MS	F	P
Regression	6	197439.0	197439.0	32907.0	16.1	0.000
Linear	4	122977.0	137679.0	34420.0	16.9	0.000
ON	1	66110.0	82689.0	82689.0	40.5	0.000
OFF	1	15655.0	13778.0	13778.0	6.8	0.017
IP	1	27379.0	27379.0	27379.0	13.4	0.002
Sv	1	13833.0	13833.0	13833.0	6.8	0.017
Square	2	74462.0	74462.0	37231.0	18.3	0.000
ON*ON	1	53605.0	53605.0	53605.0	26.3	0.000
OFF*OFF	1	20857.0	20857.0	20857.0	10.2	0.005
Residual Error	20	40810.0	40810.0	2041.0		
Lack-of-Fit	2	5954.0	5954.0	2977.0	1.5	0.242
Pure Error	18	34857.0	34857.0	1936.0		
Total	26	238249.0				

A single response optimization was performed to determine the best μ-WEDM cutting parameters that lead to reducing the Sa by using the gradient algorithm (individual desirability), as explained in Equations 3.2 to 3.6, which are provided by the surface response methodology in the Minitab software.

Figure 3.6 shows the optimum μ-WEDM cutting parameters for the minimum Mh, followed by the extracted result being compared with the PSO algorithm results for the same Sa regression model to obtain an accurate result. The PSO is explained by Equations 3.7 to 3.14.

Table 3.11 shows the comparative results of the optimum μ-WEDM cutting parameters for the minimum Mh. However, it was found that there is a slight difference in the Mh values and the optimum cutting parameter values are almost negligible between the two algorithms.

Table 3.11 shows the comparative results of W-WEDM optimum cutting parameters for the minimum Mh. Although the values of the optimum cutting parameters are identical between the two algorithms, the Mh values were found to be slightly different.

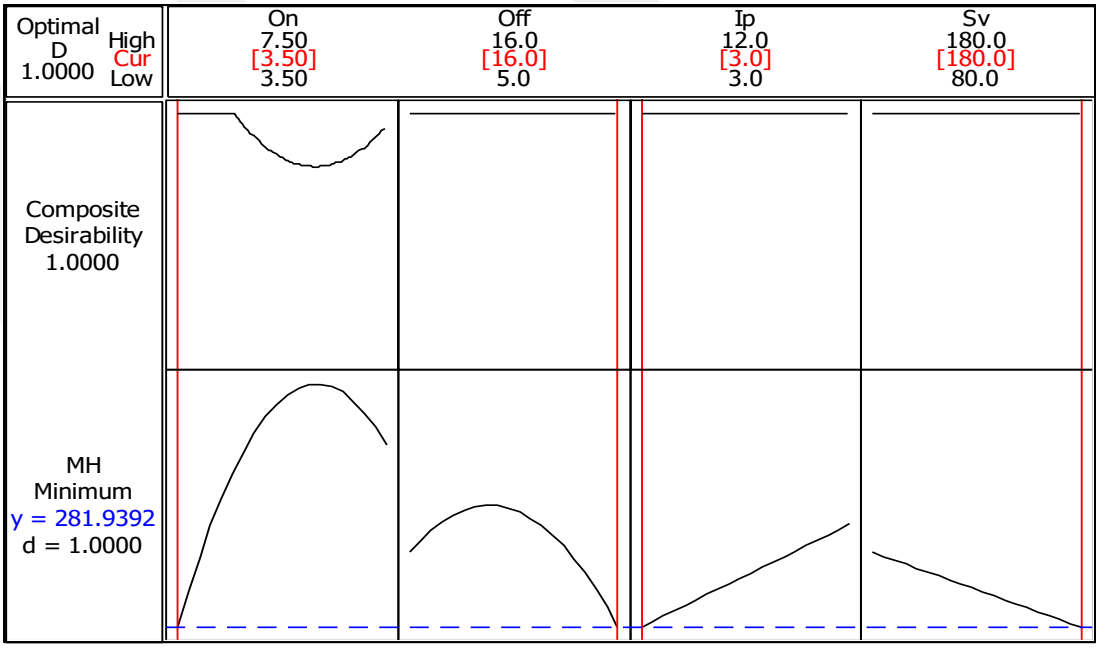

Figure 3. 6 Optimum μ-WEDM cutting parameters for minimum Mh

Table 3 11 Optimum μ-WEDM cutting parameters for minimum Mh

parameters	d. index = 1.0	PSO
Pulse on time (Ton) μs	3.5	3.5
Pulse off time(Toff) μs	16	16
Peak current (Ip) A	3	3
Servo voltage (Sv) V	180	180
μ hardness (Vikers)	281.9392	281.93919

3.4.6 Multi-Responses Optimization

A multi-response optimization was performed to determine the best μ-WEDM cutting parameters that lead to satisfying all of the response targets simultaneously.

Initially, regression models were extracted for each individual response. Together, these models were used to optimize multiple responses to obtain the best μ-WEDM cutting parameters, as explained in 3.4.1 to 3.4.5.

A multi-response optimization was carried out by applying PSO and gradient algorithm, as explained in Equations 3.2 to 3.14. Table 3.12 shows the entered input values for the multiple response optimization for the gradient algorithm. Weight and importance factors were selected to achieve the highest desirability function index, while the range of responses was selected based on the observation data.

Table 3 12 Gradient Algorithm Initial Data

parameters	Goal	Lower	Target	Upper	Weight	Import
MH	Minimum	400	400	690	1	1
W.L.T	Minimum	2.1	2.1	6	1	1
Sa	Minimum	0.2	0.2	0.39	0.1	1
KERF	Minimum	0.22	0.22	0.3	0.1	1
MRR	Maximum	0.06	0.6	0.6	0.1	1

Figure 3.7 shows the optimum μ-WEDM cutting parameters for multi responses, which are μ-hardness (Mh), white layer thickness (W.L.T.), surface roughness (Sa), kerf variation and metal removal rate (MRR).

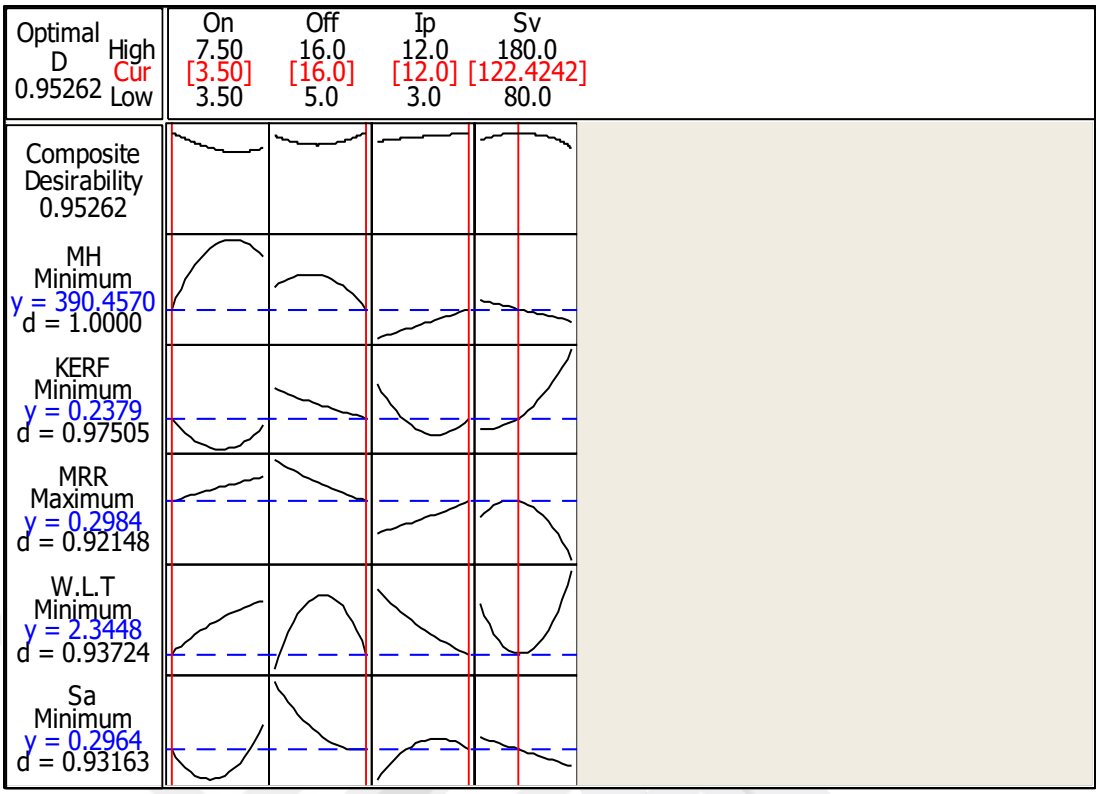

Figure 3. 7 Optimum µ-WEDM cutting parameters for multi-response using the gradient algorithm

The extracted result using the gradient algorithm was compared with the particle swarm optimization algorithm (PSO) results for the same responses to obtain an accurate result. The fitness equation that was used for the multi-responses optimization by the PSO is given by:

$$\min(Y) = w1 * Kerf + w2 * WLT + w3 * Sa + w4 * Mh - w5 * MRR \qquad (3.20)$$

where, min(Y) is the minimum fitness equation predicted value, kerf, WLT, Sa, Mh, and MRR are the response regression models, and w1 = w2 = w3 = w5 = 1.0 and w4 = 0.01 are the weights assigned to each response's regression model. Table 3.13 shows the comparative results of the optimum µ-WEDM cutting parameters for the multi-response optimization.

Table 3 13 Comparative optimum μ-WEDM cutting parameters for combined responses

parameter	* C.D of RSM = 0.95262	PSO
ON (μs)	3.5	3.5
Off (μs)	16	16
Ip (A)	12	12
Sv (v)	122.4242	128.25377

* C.D of RSM is combined desirability index by response surface methodology

Table 3.14 shows the comparative results of the predicted response values based on their μ-WEDM optimum cutting parameters. Table 3.14 shows the comparative results of the expected response values based on the regression models and WEDM optimal cutting parameters with the desired combination value of 0.953236. Although the optimum cut parameter values are somewhat compatible between both algorithms, as shown in Table 3.13, there is a very slight difference in response values.

Table 3 14 μ-WEDM optimum cutting parameters for the predicted responses by RSM and PSO

Predicted Responses	RSM C.D = 0.95262		PSO
	value	*i.d.	
MH (Vickers)	390.457	1	387.22479
W.L.T (μ m)	2.345	0.937236	2.35345
Sa (μ m)	0.296	0.931635	0.29518
KERF (mm)	0.238	0.975048	0.23821
MRR (mm3/min)	0.298	0.921481	0.29164

*i.d. is the individual desirability function index for every response.

CHAPTER 4

Conclusions and Future Works

4.1 Conclusions

In this thesis, the effect of the μ-WIDM cutting parameters on the Nitinol alloy (SMA) $Ni_{50\%}$-$Ti_{50\%}$ was studied to determine the effect of these parameters on the surface integrity of the workpiece.

The Sodick 250 lp μ-WEDM precision machine was used for cutting with 0.1 mm diameter brass cutting wire. Pilot experiments were conducted to determine the working ranges of four adjusted cutting parameters selected on the machine. Nine kerfs were then cut under different conditions of adjusted cutting parameters.

Grinding, polishing, etching and ultrasonic cleaning processes on the cross-section of the Nitinol alloy workpiece were performed to obtain clear and accurate results while measuring the kerf widths and the white layer thickness and its composition using a scan electron microscope (SEM) supported with an EDX unit.

The number of experiments (DOE) was designed based on the Taguchi orthogonal array (L_{27}) for different conditions of cutting parameters.

Kerf width measurements were taken for three different positions for each kerf while ten measurements were made for each position. In total, 30 measurements were taken for every kerf. In addition, the white layer thickness was measured in the same manner as was used with the kerf. EDX analysis was performed to study the white layer phase compositions using the EDX unit of the SEM.

The nine samples were separated using a milling machine, followed by surface roughness measurements of the machined surfaces is made using a precision confocal laser scanning microscope. μ-hardness tests were carried out using the Zwick/Roell μ-Hardness tester and the microstructural analysis was performed for each machined surface using the SEM supported by the EDX unit.

After the preparation of the Taguchi orthogonal array L_{27}, the analysis of variance was performed based on the response surface methodology to build a regression model for the kerf, surface roughness, μ-hardness, white layer thickness, and metal removal rate. An optimization analysis was performed for each response individually, followed by combining them to conduct an optimization analysis of all responses concurrently to find the optimal values of the μ-WEDM cutting parameters and their optimal response values for individual and combined optimization analyses, respectively.

The optimization analysis was performed using gradient algorithms and particle swarm optimization. The results of the algorithms were compared to obtain the highest possible accuracy.

Through the ANOVA analysis of all responses, it was found that the most effective μ-WEDM cutting parameters on the **Kerf width** were servo voltage and peak current. The most effective μ-WEDM cutting parameters on the **μ-hardness** were pulse on time and peak current. The most effective μ-WEDM cutting parameters on the **MRR** was servo voltage, pulse off time.

Also through the ANOVA analysis, it can be observed that the most effective μ-WEDM cutting parameters on the **WLT** were peak current and servo voltage and the most effective μ-WEDM cutting parameters on the **Sa** were pulse off time and peak current.

Here, it is possible to conclude that the most significant cutting parameters in the μ-WEDM process were found to be peak current and servo voltage, where the pulse off time and pulse on time are in close proportion.

Through the optimization analysis of all individual responses, it was found that the optimal cutting parametric settings that had been obtained for the μ-WEDM process to obtain better **kerf width**, which was 0.233 mm, were T_{on} = 5.64 μs, T_{off} = 16 μs, Ip = 8.73 A, and Sv = 87.07 V. The optimal cutting parametric settings that had been obtained for the μ-WEDM process to obtain better **MRR,** which was 0.564 mm^3/min, were T_{on} = 7.5 μs, T_{off} = 5 μs, Ip = 12 A, and Sv = 115.35 V. Moreover, the optimal cutting parametric settings that had been obtained for the μ-WEDM process to obtain better **WLT**, which was 2.052 μm**,** were T_{on} = 3.5 μs, T_{off} = 5 μs, Ip = 12 A, and Sv = 123.43 V. Moreover, the optimal cutting parametric settings that had been

obtained for the μ-WEDM process to obtain better **Sa,** which was 0.239 μm**,** were T_{on} = 5.19 μs, T_{off} = 15.22 μs, Ip = 3 A, and Sv = 180 V. The optimal cutting parametric settings that had been obtained for the μ-WEDM process to obtain better **Mh,** which was 281.94 Vickers, were T_{on} = 3.5 μs, T_{off} = 16 μs, Ip = 3 A, and Sv = 180 V.

In addition, a combined multi-response optimization analysis was performed to find the best cut parameters setting for μ-WEDM for the best surface integrity of the Nitinol alloy sample were T_{on} = 3.5 μs, T_{off} = 16 μs, Ip = 12 A, and Sv = 122.42 V, and Mh = 390.46 Vickers, white layer thickness = 2.345 μm, surface roughness = 0.296 μm, kerf = 0.238 mm and metal removal rate = 0.298 (mm^3/min).

4.2 Future Works

Few works have dealt with the topics of the effect of μ-WEDM cutting parameters on machined surfaces of Nitinol alloys (shape memory alloys). There is an urgent need for more extensive studies to study significant parameters such as cutting wire vibration, cutting wire type and other dielectric fluid types.

In addition, there is a need to conduct other experiments to study the machined surface parameters that play an important role in improving surface integrity, such as residual stress using X-ray diffraction, thermal fatigue life, heat-affected zones using the backscattering electrons unit of the SEM to studying its grain size.

REFRENCES

[1] K. E. Wilkes and P. K. Liaw, "The fatigue behavior of shape-memory alloys," *JOM*, vol. 52, no. 10, pp. 45-51, 2000.

[2] M. Manjaiah, S. Narendranath, and S. Basavarajappa, "Review on non-conventional machining of shape memory alloys," *Transactions of Nonferrous Metals Society of China*, vol. 24, no. 1, pp. 12-21, 2014.

[3] H. Lin, K. Lin, and Y. Chen, "A study on the machining characteristics of TiNi shape memory alloys," *Journal of materials processing technology*, vol. 105, no. 3, pp. 327-332, 2000.

[4] M. H. Elahinia, *Shape memory alloy actuators: design, fabrication, and experimental evaluation*. John Wiley & Sons, 2016.

[5] J. Al-Haidary and S. Al-Khatiab, "Manufacturing and characterization of dental shape memory alloy," *Materials Science and Engineering: A*, vol. 419, no. 1-2, pp. 45-49, 2006.

[6] Y. Guo, A. Klink, C. Fu, and J. Snyder, "Machinability and surface integrity of Nitinol shape memory alloy," *CIRP Annals*, vol. 62, no. 1, pp. 83-86, 2013.

[7] M. Collado, R. Cabás, J. San Juan, and I. López-Ferreño, "Functional characterization of a novel shape memory alloy," *Journal of materials engineering and performance*, vol. 23, no. 7, pp. 2321-2326, 2014.

[8] O. Adiguzel, "Smart materials and the influence of atom sizes on martensite microstructures in copper-based shape memory alloys," *Journal of materials processing technology*, vol. 185, no. 1-3, pp. 120-124, 2007.

[9] D. L. Schodek, *Smart materials and new technologies: for the architecture and design professions*. Architectural press, 2005.

[10] N. Morgan, "Medical shape memory alloy applications—the market and its products," *Materials Science and Engineering: A*, vol. 378, no. 1-2, pp. 16-23, 2004.

[11] G. B. Kauffman and I. Mayo, "The story of nitinol: the serendipitous discovery of the memory metal and its applications," *The chemical educator*, vol. 2, no. 2, pp. 1-21, 1997.

[12] D. J. Hartl and D. C. Lagoudas, "Aerospace applications of shape memory alloys," *Proceedings of the Institution of Mechanical Engineers, Part G: Journal of Aerospace Engineering*, vol. 221, no. 4, pp. 535-552, 2007.

[13] T. Duerig, A. Pelton, and D. Stöckel, "An overview of nitinol medical applications," *Materials Science and Engineering: A*, vol. 273, pp. 149-160, 1999.

[14] A. Kneissl, E. Unterweger, M. Bruncko, G. Lojen, K. Mehrabi, and H. Scherngell, "Microstructure and properties of NiTi and CuAlNi shape memory alloys," *Metalurgija*, vol. 14, no. 2, pp. 89-100, 2008.

[15] T. W. Duerig, K. Melton, and D. Stöckel, *Engineering aspects of shape memory alloys*. Butterworth-Heinemann, 2013.

[16] K. Weinert and V. Petzoldt, "Machining of NiTi based shape memory alloys," *Materials Science and Engineering: A*, vol. 378, no. 1-2, pp. 180-184, 2004.

[17] D. Ulutan and T. Ozel, "Machining induced surface integrity in titanium and nickel alloys: A review," *International Journal of Machine Tools and Manufacture,* vol. 51, no. 3, pp. 250-280, 2011.
[18] Y. Kaynak, H. Karaca, R. Noebe, and I. Jawahir, "Analysis of tool-wear and cutting force components in dry, preheated, and cryogenic machining of NiTi shape memory alloys," *Procedia CIRP,* vol. 8, pp. 498-503, 2013.
[19] S. Daneshmand, E. F. Kahrizi, E. Abedi, and M. M. Abdolhosseini, "Influence of machining parameters on electro discharge machining of NiTi shape memory alloys," *Int. J. Electrochem. Sci,* vol. 8, no. 3, pp. 3095-3104, 2013.
[20] A. Lotfi, S. Daneshmand, and S. A. Nazari, "The effect of operational cutting parameters in the wire electro discharge machining (WEDM) on micro hardness of alloy surface layer," *International Journal of Advanced Design and Manufacturing Technology,* vol. 2, no. 4, pp. 51-58, 2011.
[21] C.-P. Lin, K.-M. Hsiao, and C.-C. Wu, "Parameter analysis and optimization of electrolytic in-process dressing grinding on ceramics," *Journal of Marine Science and Technology,* vol. 11, no. 2, pp. 104-112, 2003.
[22] M. Haddad and A. F. Tehrani, "Material removal rate (MRR) study in the cylindrical wire electrical discharge turning (CWEDT) process," *Journal of Materials Processing Technology,* vol. 199, no. 1-3, pp. 369-378, 2008.
[23] S. Chen, S. Hsieh, H. Lin, M. Lin, and J. Huang, "Electrical discharge machining of a NiAlFe ternary shape memory alloy," *Journal of alloys and compounds,* vol. 464, no. 1-2, pp. 446-451, 2008.
[24] A. Kumar, V. Kumar, and J. Kumar, "Multi-response optimization of process parameters based on response surface methodology for pure titanium using WEDM process," *The International Journal of Advanced Manufacturing Technology,* vol. 68, no. 9-12, pp. 2645-2668, 2013.
[25] L. Zhu, Y. Guan, Y. Wang, Z. Xie, J. Lin, and J. Zhai, "Influence of process parameters of ultrasonic shot peening on surface roughness and hydrophilicity of pure titanium," *Surface and Coatings Technology,* vol. 317, pp. 38-53, 2017.
[26] A. Pukasiewicz, H. De Boer, G. Sucharski, R. Vaz, and L. Procopiak, "The influence of HVOF spraying parameters on the microstructure, residual stress and cavitation resistance of FeMnCrSi coatings," *Surface and Coatings Technology,* vol. 327, pp. 158-166, 2017.
[27] C. Prakash and M. Uddin, "Surface modification of β-phase Ti implant by hydroaxyapatite mixed electric discharge machining to enhance the corrosion resistance and in-vitro bioactivity," *Surface and Coatings Technology,* vol. 326, pp. 134-145, 2017.
[28] B. Mordyuk, G. Prokopenko, K. Grinkevych, N. Piskun, and T. Popova, "Effects of ultrasonic impact treatment combined with the electric discharge surface alloying by molybdenum on the surface related properties of low-carbon steel G21Mn5," *Surface and Coatings Technology,* vol. 309, pp. 969-979, 2017.
[29] M. Mello, M. Taipina, G. Rabelo, A. Cremasco, and R. Caram, "Production and characterization of TiO2 nanotubes on Ti-Nb-Mo-Sn system for biomedical applications," *Surface and Coatings Technology,* vol. 326, pp. 126-133, 2017.

[30] G. Liu, C. Huang, B. Zou, X. Wang, and Z. Liu, "Surface integrity and fatigue performance of 17-4PH stainless steel after cutting operations," *Surface and Coatings Technology*, vol. 307, pp. 182-189, 2016.
[31] S. Javadi, M. Ghoranneviss, R. Rawat, and A. S. Elahi, "Topographical, structural and hardness changes in surface layer of stainless steel-AISI 304 irradiated by fusion-relevant high energy deuterium ions and neutrons in a low energy plasma focus device," *Surface and Coatings Technology*, vol. 313, pp. 73-81, 2017.
[32] S. Kuriakose and M. Shunmugam, "Characteristics of wire-electro discharge machined Ti6Al4V surface," *Materials Letters*, vol. 58, no. 17-18, pp. 2231-2237, 2004.
[33] S. Daneshmand, R. Hessami, and H. Esfandiar, "Investigation of wire electro discharge machining of Nickel-Titanium shape memory alloys on surface roughness and MRR," *Life Science Journal*, vol. 9, no. 4, pp. 2904-2909, 2012.
[34] A. Alidoosti, A. Ghafari-Nazari, F. Moztarzadeh, N. Jalali, S. Moztarzadeh, and M. Mozafari, "Electrical discharge machining characteristics of nickel–titanium shape memory alloy based on full factorial design," *Journal of intelligent Material systems and Structures*, vol. 24, no. 13, pp. 1546-1556, 2013.
[35] R. Rao and P. Pawar, "Modelling and optimization of process parameters of wire electrical discharge machining," *Proceedings of the Institution of Mechanical Engineers, Part B: Journal of Engineering Manufacture*, vol. 223, no. 11, pp. 1431-1440, 2009.
[36] Y. Fan, J. Bai, C. Li, and W. Xu, "Research on precision pulse power technology of WEDM," *Procedia CIRP*, vol. 6, pp. 267-273, 2013.
[37] Y. Kaynak, H. Karaca, and I. Jawahir, "Sustainability evaluation in machining of NiTi shape memory alloy," in *1st international Conference on Sustainable Life in Manufacturing (SLIM 2010)*, 2010, pp. 40-47.
[38] Y. Kaynak, H. Karaca, and I. Jawahir, "Cryogenic machining of NiTi shape memory alloy," in *6th International Conference and Exhibition on Design and Production of Machines and Dies/Molds*, 2011, pp. 23-26.
[39] M. Es-Souni, M. Es-Souni, and H. Fischer-Brandies, "On the properties of two binary NiTi shape memory alloys. Effects of surface finish on the corrosion behaviour and in vitro biocompatibility," *Biomaterials*, vol. 23, no. 14, pp. 2887-2894, 2002.
[40] N. Tosun, C. Cogun, and G. Tosun, "A study on kerf and material removal rate in wire electrical discharge machining based on Taguchi method," *Journal of Materials Processing Technology*, vol. 152, no. 3, pp. 316-322, 2004/10/30/ 2004.
[41] S. Chen, S. Hsieh, H. Lin, M. Lin, and J. Huang, "Electrical discharge machining of TiNiCr and TiNiZr ternary shape memory alloys," *Materials Science and Engineering: A*, vol. 445, pp. 486-492, 2007.
[42] A. Majumder, P. K. Das, A. Majumder, and M. Debnath, "An approach to optimize the EDM process parameters using desirability-based multi-objective PSO," *Production & Manufacturing Research*, vol. 2, no. 1, pp. 228-240, 2014.
[43] I. Puertas, C. Luis, and L. Alvarez, "Analysis of the influence of EDM parameters on surface quality, MRR and EW of WC–Co," *Journal of Materials Processing Technology*, vol. 153, pp. 1026-1032, 2004.

[44] F. S. Al-Anzi and A. Allahverdi, "A self-adaptive differential evolution heuristic for two-stage assembly scheduling problem to minimize maximum lateness with setup times," *European Journal of Operational Research,* vol. 182, no. 1, pp. 80-94, 2007.
[45] A. Chatterjee, R. Chatterjee, F. Matsuno, and T. Endo, "Neuro-fuzzy state modeling of flexible robotic arm employing dynamically varying cognitive and social component based PSO," *Measurement,* vol. 40, no. 6, pp. 628-643, 2007.
[46] P. Fourie and A. A. Groenwold, "The particle swarm optimization algorithm in size and shape optimization," *Structural and Multidisciplinary Optimization,* vol. 23, no. 4, pp. 259-267, 2002.
[47] M. Cunningham, P. Higgins, and J. Browne, "A decision support tool for planning bills-of-material," *Production Planning & Control,* vol. 7, no. 3, pp. 312-328, 1996.
[48] J. Júnior *et al.*, "Multi-Objective Optimization Techniques to Solve the Economic Emission Load Dispatch Problem Using Various Heuristic and Metaheuristic Algorithms," 2018, pp. 13-32.
[49] N. Baskar, P. Asokan, G. Prabhaharan, and R. Saravanan, "Optimization of machining parameters for milling operations using non-conventional methods," *The International Journal of Advanced Manufacturing Technology,* vol. 25, no. 11-12, pp. 1078-1088, 2005.
[50] J. E. R. Dhas and S. Kumanan, "Optimization of parameters of submerged arc weld using non conventional techniques," *Applied soft computing,* vol. 11, no. 8, pp. 5198-5204, 2011.
[51] Q. Bai, "Analysis of particle swarm optimization algorithm," *Computer and information science,* vol. 3, no. 1, p. 180, 2010.
[52] M. Clerc, "The swarm and the queen: towards a deterministic and adaptive particle swarm optimization," in *Proceedings of the 1999 congress on evolutionary computation-CEC99 (Cat. No. 99TH8406)*, 1999, vol. 3, pp. 1951-1957: IEEE.
[53] M. Vishwakarma, V. Parashar, and V. Khare, "Optimization and regression analysis of surface roughness for electric discharge machining of EN-19 alloy steel using tungsten copper electrode," *International Journal of Engineering Research and Applications,* vol. 2, no. 6, pp. 785-792, 2012.
[54] S. S. Kumar, F. Erdemir, T. Varol, S. T. Kumaran, M. Uthayakumar, and A. Canakci, "Investigation of WEDM process parameters of Al–SiC–B4C composites using response surface methodology," *International Journal of Lightweight Materials and Manufacture,* 2019.
[55] N. Sharma, R. Khanna, and R. D. Gupta, "WEDM process variables investigation for HSLA by response surface methodology and genetic algorithm," *Engineering science and technology, an international journal,* vol. 18, no. 2, pp. 171-177, 2015.

APPENDIX A

PSO'S MATH LAB CODE

```
%*********************************************************************
% Optimization of μ-wedm affected parameters of Nitinol alloy cutting processes
%     Using particle swarm optimization - all of three methods
%                  (PSO-original, IW, and CF)
%*********************************************************************
clc;
clear;
clear all;
close all;
tic;
%----------------------------------------------------------------------
%  μ-wedm parameters values and program inputs----------------------start
%----------------------------------------------------------------------
m=4;    % number of μ-wedm parameters
n=27;   % number of μ-wedm experiments
LB=[3.5 5 3 80]; %lower bounds of μ-wedm parameters [ Ton  Toff  Ip  Sv  ]
UB=[7.5 16 12 180];%upper bounds of μ-wedm parameters [ Ton  Toff  Ip  Sv  ]
wmax=0.9;         % maximum inertia weight
wmin=0.4;         % minimum inertia weight
c1=2;             % cognitive factor ( indviual parameter )
c2=2;             % social factor ( group parameter )
                % c1+c2 <= 4
maxite=2000;      % set maximum number of iteration
maxrun=5;         % set maximum number of times need to be run
%----------------------------------------
imwlt=1;   % (1,0.1,0.01) importance value of white recast layer for muli-objective
analysis
immrr=1;   % importance value of MRR for muli-objective analysis
imkerf=1;  % importance value of KERF for muli-objective analysis
imsa=1;    % importance value of Surface Roughness for muli-objective analysis
immh=0.01; %(0.001,0.01) importance value of micro hardness for muli-objective
analysis
% note:
% if you do not like to calculate micro-hardness put immh=0 rather
% than leave immh=0.01 becuase if it is not all values of kerf, mrr, wlt,
% and sa are at the range (x.xxxx) and mh is at the range (xxx.xx)this will
% cause calculating errors during optimizations proccesses.
```

```
%-------------------------------------------------------------------------
% The best input iportance values of Nitinol optimization are :
% imwlt=0.1;   % importance value of white recast layer for muli-objective analysis
% immrr=1;   % importance value of MRR for muli-objective analysis
% imkerf=1;  % importance value of KERF for muli-objective analysis
% imsa=1;    % importance value of Surface Roughness for muli-objective analysis
% immh=0.001; % importance value of micro hardness for muli-objective analysis
%-------------------------------------------------------------------------
psotype=3;        % choose (1) for pso-original.
                  % choose (2) for pso-inertia weight.
                  % choose (3) for pso-constriction factor.
                  % rather than the program well be terminated.
%-------------------------------------------------------------------------
%  µ-wedm parameters values and program inputs--------------------------end
%-------------------------------------------------------------------------
importance.imw=imwlt;
importance.imm=immrr;
importance.imk=imkerf;
importance.ims=imsa;
importance.imh=immh;
c=c1+c2;  % c1+c2 <= 4
k=2/abs(2-c-sqrt(c^2-4*c)); % constriction factor "kaba"
% pso main program-----------------------------------------------------start
for run=1:maxrun
% pso initialization---------------------------------------------start
%if run > 1
%    x0=x;
%else
for i=1:n
for j=1:m
%x0(i,j)=round(LB(j)+rand*(UB(j)-LB(j)));
x0(i,j)=(LB(j)+rand*(UB(j)-LB(j)));
end
end
%end
x=x0;     % initial population
v=0.1*x0; % initial velocity
for i=1:n
f0(i,1)=ofun(x0(i,:),importance);
end
[fmin0,index0]=min(f0);
pbest=x0;          % initial pbest
gbest=x0(index0,:); % initial gbest
% pso initialization-----------------------------------------------end
% pso algorithm-----------------------------------------------------start
ite=1;
tolerance=1;
while ite<=maxite && tolerance>10^-12
w=wmax-(wmax-wmin)*ite/maxite; % update inertial weight
% pso velocity updates
```

```
for i=1:n
for j=1:m
% type of algorithm----------------------------------------------start
   if psotype==1
% original algorithm----------------------------------------------start
v(i,j)=(v(i,j)+c1*rand*(pbest(i,j)-x(i,j))...
      +c2*rand*(gbest(1,j)-x(i,j)));
% original algorithm----------------------------------------------end
elseif psotype==2
% inertia weight algorithm----------------------------------------start
v(i,j)=w*v(i,j)+c1*rand*(pbest(i,j)-x(i,j))...
      +c2*rand*(gbest(1,j)-x(i,j));
% inrtia weight algorithm----------------------------------------end
elseif psotype==3
% constriction factor algorithm----------------------------------start
v(i,j)=k*(v(i,j)+c1*rand*(pbest(i,j)-x(i,j))...
      +c2*rand*(gbest(1,j)-x(i,j)));
% constriction factor algorithm----------------------------------end
   else
       clear;
       clc;
disp(sprintf('the program has been terminated, please choose correct PSO-method'));
end
end
% pso position update
for i=1:n
for j=1:m
x(i,j)=x(i,j)+v(i,j);
end
end
% handling boundary violations
for i=1:n
for j=1:m
if x(i,j)<LB(j)
x(i,j)=LB(j);
elseif x(i,j)>UB(j)
x(i,j)=UB(j);
end
end
end
% evaluating fitness
for i=1:n
f(i,1)=ofun(x(i,:),importance);
end
% updating pbest and fitness
for i=1:n
if f(i,1)<f0(i,1)
   pbest(i,:)=x(i,:);
f0(i,1)=f(i,1);
end
```

```
end
[fmin,index]=min(f0); % finding out the best particle
ffmin(ite,run)=fmin;  % storing best fitness
ffite(run)=ite;       % storing iteration count
% updating gbest and best fitness
if fmin<fmin0
gbest=pbest(index,:);
fmin0=fmin;
end
% calculating tolerance
if ite>100;
tolerance=abs(ffmin(ite-100,run)-fmin0);
end
% ----------------------------------------------------
ffmin_wlt(ite,run)=ofun_wlt(gbest);
ffmin_mrr(ite,run)=ofun_mrr(gbest);
ffmin_kerf(ite,run)=ofun_kerf(gbest);
ffmin_sa(ite,run)=ofun_sa(gbest);
ffmin_mh(ite,run)=ofun_mh(gbest);
% ----------------------------------------------------
% (A)-
%ite=ite+1; % " i think here is not good positon for increasing iteration
        %   becuase we still under run of  " i "
        %   it is better for short time run, and evry i cuase of 28 iterations

end  % end of "i" after while command at pso velocity updates
% (B)-
ite=ite+1;  %  it will take long time becuase evry i leds to 1 iteration
          %  only
end % end of iteration. " while"
% pso algorithm----------------------------------------------------end
gbest;
fvalue=ofun(gbest,importance);
fff(run)=fvalue;
rgbest(run,:)=gbest;
end  % end of run.
% pso main program----------------------------------------------------end
% pso printing results ----------------------------------------------start
if psotype==1
disp(sprintf('\nThese results are obtained using PSO-original method\n'));
elseif psotype==2
disp(sprintf('\nThese results are obtained using PSO-inertia weight method\n'));
elseif psotype==3
disp(sprintf('\nThese results are obtained using PSO-constriction factor method\n'));
end
[bestfun,bestrun]=min(fff);
best_variables=rgbest(bestrun,:);
importance.WLT=ofun_wlt(best_variables);
importance.MRR=ofun_mrr(best_variables);
importance.KERF=ofun_kerf(best_variables);
```

```
importance.SA=ofun_sa(best_variables);
importance.MH=ofun_mh(best_variables);
rq_t=toc;
disp(sprintf(' Required time was = %5.2f%s,\n The number of iterations at last
program run were = %5.0f%s.\n',...
        rq_t,' seconds',ite,' times'));
disp(sprintf(' Number of program runs = %5.2f%s,\n Tolerance was = %e.\n',...
        run,' times',tolerance));
disp(sprintf('**********************************************************'));
resultfun(importance,best_variables);
% pso printing results ----------------------------------------------end
% PSO convergence characteristic plotting --------------------------start
drawings.ffite=ffite;
drawings.bestrun=bestrun;
drawings.ffmin=ffmin;
drawings.ffmin_wlt=ffmin_wlt;
drawings.ffmin_kerf=ffmin_kerf;
drawings.ffmin_mrr=ffmin_mrr;
drawings.ffmin_sa=ffmin_sa;
drawings.ffmin_mh=ffmin_mh;
plotting(importance,drawings);
% PSO convergence characteristic plotting --------------------------end
%#########################################################################
%-------------------------------------------------------------------------------------------end


function f=ofun(x,importance)
% multi-objective optimization function (minimization)
%W.L.T FUNCTION-----------------------------------------------------
f_wlt=ofun_wlt(x);
%MRR FUNCTION-------------------------------------------------------
f_mrr=ofun_mrr(x);
%KERF FUNCTION------------------------------------------------------
f_kerf=ofun_kerf(x);
%SA FUNCTION--------------------------------------------------------
f_sa=ofun_sa(x);
%micro hardness FUNCTION-------------------------------------------------------
f_mh=ofun_mh(x);
%-------------------------------------------------------------------
f=(f_wlt*importance.imw)+(f_mh*importance.imh)+(f_kerf*importance.imk)+ ...
  (f_sa*importance.ims)-(f_mrr*importance.imm);
%-------------------------------------------------------------------

function fkerf=ofun_kerf(x)
% objective function (minimization)
% KERF FUNCTION-----------------------------------------------------------
fkerf= 0.271249-0.00648521*x(1)-3.19560E-04*x(2)-0.00232323*x(3)-1.37654E-
04*x(4)+0.000574513*x(1)^2+4.64791E-
06*x(2)^2+0.000132975*x(3)^2+7.86001E-07*x(4)^2;
```

```
function fmh=ofun_mh(x)
% objective function (minimization)
%micro hardness FUNCTION----------------------------------------------------
fmh= (-507.860)+314.022*x(1)+36.2980*x(2)+8.51058*x(3)-0.554444*x(4)-
25.4667*x(1)^2-1.96801*x(2)^2;


function fmrr=ofun_mrr(x)
% objective function (maximaization)
%MRR FUNCTION----------------------------------------------------------------
fmrr=(-0.435038)+0.0327070*x(1)-
0.0213667*x(2)+0.00942807*x(3)+0.0128029*x(4)-7.22974E-
04*x(1)^2+0.000308625*x(2)^2+0.000310072*x(3)^2-5.56803E-05*x(4)^2;


function fsa=ofun_sa(x)
% objective function (minimization)
%Sa FUNCTION-----------------------------------------------------------
fsa= 0.554337-0.0786443*x(1)-0.0146251*x(2)+0.0156574*x(3)-2.12111E-
04*x(4)+0.00757296*x(1)^2+0.000479596*x(2)^2-8.75926E-04*x(3)^2;


function fwlt=ofun_wlt(x)
% objective function (minimization)
%W.L.T FUNCTION--------------------------------------------------------------
fwlt =6.13701+0.577222*x(1)+0.850824*x(2)-0.236046*x(3)-0.116228*x(4)-
0.0309423*x(1)^2-0.0392519*x(2)^2+0.00712647*x(3)^2+0.000469543*x(4)^2;


function fpol=plotting(importance,drawings)
% PSO convergence characteristic-----------------------------------start
%if importance.imw~=0 && importance.imk~=0 && importance.imm~=0 &&
importance.ims~=0
subplot(2,3,1);
plot(drawings.ffmin(1:drawings.ffite(drawings.bestrun),drawings.bestrun),'-k');
xlabel('Iteration');
ylabel('Fitness function value');
title('PSO convergence characteristic')
grid on
%end
% PSO convergence characteristic  of WLT ----------------------------start
if importance.imw~=0
subplot(2,3,2);
plot(drawings.ffmin_wlt(1:drawings.ffite(drawings.bestrun),drawings.bestrun),'-k');
xlabel('Iteration');
ylabel('WLT function value');
title('PSO convergence characteristic of WLT')
grid on
end
```

```
% PSO convergence characteristic  of WLT ----------------------------end
% PSO convergence characteristic  of KERF ---------------------------start
if importance.imk~=0
subplot(2,3,3);
plot(drawings.ffmin_kerf(1:drawings.ffite(drawings.bestrun),drawings.bestrun),'-k');
xlabel('Iteration');
ylabel('KERF function value');
title('PSO convergence characteristic of KERF')
grid on
end
% PSO convergence characteristic  of KERF ---------------------------end
% PSO convergence characteristic  of MRR ----------------------------start
if importance.imm~=0
subplot(2,3,4);
plot(drawings.ffmin_mrr(1:drawings.ffite(drawings.bestrun),drawings.bestrun),'-k');
xlabel('Iteration');
ylabel('MRR function value');
title('PSO convergence characteristic of MRR')
grid on
end
% PSO convergence characteristic  of MRR ----------------------------end
% PSO convergence characteristic  of Sa -----------------------------start
if importance.ims~=0
subplot(2,3,5);
plot(drawings.ffmin_sa(1:drawings.ffite(drawings.bestrun),drawings.bestrun),'-k');
xlabel('Iteration');
ylabel('Sa function value');
title('PSO convergence characteristic of Sa')
grid on
end
% PSO convergence characteristic  of Sa -----------------------------end
% PSO convergence characteristic  of micro-hardness -----------------start
if importance.imh~=0
subplot(2,3,6);
plot(drawings.ffmin_mh(1:drawings.ffite(drawings.bestrun),drawings.bestrun),'-k');
xlabel('Iteration');
ylabel('micro-hardness function value');
title('PSO convergence characteristic of micro-hardness')
grid on
end
% PSO convergence characteristic  of micro-hardness------------------end
% PSO convergence characteristic-------------------------------------end


function resfun=resultfun(importance,best_variables)
% sub fuction to print out the results ------------------------------------start
disp(sprintf(' Optimum μ-wedm parameters------------------------------\n'));
disp(sprintf(' 1)-Pulse on time (Ton)  = %2.5f%s,\n 2)-Pulse off time(Toff) =
%2.5f%s,\n 3)-Peak current (Ip)    = %2.5f%s,\n 4)-Servo voltage (Sv)   =
%3.5f%s\n',...
```

```
        best_variables(1),' µs',best_variables(2),' µs',best_variables(3),'
A',best_variables(4),' V'));
ns=0;
disp(sprintf(' The responses values based on Optimum µ-wedm parameters analysis
by PSO are:\n'));
if importance.imw~=0
ns=ns+1;
disp(sprintf(' %d%sWhite Layer Thickness     = %2.5f%s.',ns,')-',importance.WLT,'
microns'));
end
if importance.ims~=0
ns=ns+1;
disp(sprintf(' %d%ssurface roughness (Sa)    = %2.5f%s.',ns,')-',importance.SA,'
microns'));
end
if importance.imm~=0
ns=ns+1;
disp(sprintf(' %d%sMetal Removed Rate ( MRR )= %2.5f%s.',ns,')-
',importance.MRR,' mm3/min'));
end
if importance.imk~=0
ns=ns+1;
disp(sprintf(' %d%sKerf Width                = %2.5f%s.',ns,')-',importance.KERF,'
mm'));
end
if importance.imh~=0
ns=ns+1;
disp(sprintf(' %d%smicro-hardness            = %2.5f%s.',ns,')-',importance.MH,'
Vickers'));
end
disp(sprintf('\n**********************************************************'));
```